

Quasiparticle cooling algorithms for quantum many-body state preparation

Jerome Lloyd,¹ Alexios Michailidis,^{1,2} Xiao Mi,³ Vadim Smelyanskiy,³ and Dmitry A. Abanin^{3,4}

¹*Department of Theoretical Physics, University of Geneva, Geneva, Switzerland*

²*PlanQC GmbH, Lichtenbergstr. 8, 85748 Garching, Germany*

³*Google Quantum AI, Santa Barbara CA, USA*

⁴*Department of Physics, Princeton University, Princeton NJ 08544, USA*

(Dated: 19th April 2024)

Probing correlated states of many-body systems is one of the central tasks for quantum simulators and processors. A promising approach to state preparation is to realize desired correlated states as steady states of engineered dissipative evolution. A recent experiment with a Google superconducting quantum processor [X. Mi *et al.*, Science 383, 1332 (2024)] demonstrated a cooling algorithm utilizing auxiliary degrees of freedom that are periodically reset to remove quasiparticles from the system, thereby driving it towards the ground state. We develop a kinetic theory framework to describe quasiparticle cooling dynamics, and employ it to compare the efficiency of different cooling algorithms. In particular, we introduce a protocol where coupling to auxiliaries is modulated in time to minimize heating processes, and demonstrate that it allows a high-fidelity preparation of ground states in different quantum phases. We verify the validity of the kinetic theory description by an extensive comparison with numerical simulations of a 1d transverse-field Ising model using a solvable model and tensor-network techniques. Further, the effect of noise, which limits efficiency of variational quantum algorithms in near-term quantum processors, can be naturally described within the kinetic theory. We investigate the steady state quasiparticle population as a function of noise strength, and establish maximum noise values for achieving high-fidelity ground states. This work establishes quasiparticle cooling algorithms as a practical, robust method for many-body state preparation on near-term quantum processors.

I. INTRODUCTION

One of the central challenges for quantum simulation is to find reliable algorithms to prepare desired entangled quantum many-body states. In particular, preparing low-energy states of a given many-body Hamiltonian is an essential task for probing quantum dynamics, modeling correlated quantum materials, and for quantum chemistry applications of quantum computers [1–4]. Classical tasks such as high-dimensional optimization problems can also be formulated in terms of finding ground states of appropriate Hamiltonians [5, 6]. A number of quantum algorithms for preparing ground states of many-body Hamiltonians have been proposed [7–12].

Two important classes of low-energy state-preparation protocols employed in experiments with noisy intermediate-scale quantum (NISQ) devices [13] are: (i) *adiabatic* protocols [9, 14], which rely on the adiabatic theorem and a slow variation of Hamiltonian parameters, and have been widely used in analogue quantum simulators such as ultracold atoms [15, 16] and Rydberg atom arrays [17, 18]; (ii) *variational* methods [19–21], suitable for digital quantum simulators, in which the target state is prepared by applying a variational quantum circuit to a simple initial state (e.g. a product state).

The unitary state-preparation protocols on NISQ processors are hindered by the presence of intrinsic decoherence. Such protocols have no native mechanism to remove excitations, so decoherence will eventually thermalize the system to a trivial state, e.g. a fully mixed state. This restricts the size of feasible circuits and limits the duration for which a quantum state can be stored on the

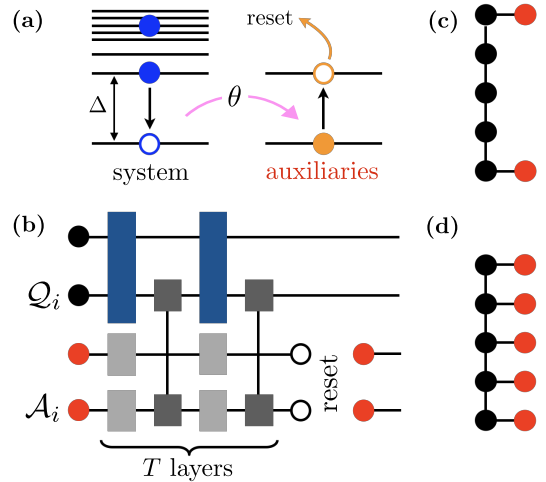


Figure 1. (a) Schematic mechanism of quasiparticle cooling: quasiparticles in the system, with energy above the system gap Δ , are resonantly transferred to auxiliary qubits, which are then reset to ground state, removing entropy and energy from the system. (b) Digital quantum circuit used in reset protocol: a system of N_S qubits Q_i is coupled to an auxiliary bath of N_A qubits A_i . Unitary evolution under system, auxiliary, and interaction gates is applied, and repeated T times, followed by the reset of auxiliaries. This cooling cycle is repeated until the system converges to its steady state. (c) Edge cooling setup. (d) Bulk cooling setup, $N_A = N_S$.

device [22, 23]. Further, using variational circuits to prepare complex quantum states may be challenging due to flat optimization landscapes (‘barren plateaus’) [24–26].

A fundamentally different approach is to prepare

many-body states as steady states of engineered dissipative evolution [27]. Because the dissipation directly competes with the decoherence effects, such state preparation methods can partially overcome the difficulties posed by noise. However, understanding which class of experimentally realisable dissipators can give rise to interesting quantum correlated steady states is a highly non-trivial question that has attracted much historic and recent interest [28–34]. In particular, specific protocols that involve *local* engineered dissipation for frustration-free Hamiltonians (a restricted but important class of models) have been proposed and implemented experimentally in few-qubit systems of trapped ions and superconducting qubits [35–37].

More recently, in an experiment [38] on the digital Google Quantum Processor, a physics-inspired cooling algorithm was demonstrated for cooling 1d and 2d quantum spin systems. In this experiment, the system evolved under a periodic (Floquet) quantum circuit specified by a unitary Floquet operator \hat{U}_S , constructed as a shallow quantum circuit of gates with finite, but small rotation angles. In this regime, the time evolution of local observables is well-approximated by a prethermal Hamiltonian H_{eff} [39]. The approximate conservation of H_{eff} stems from the suppression of heating processes, which are exponentially slow in the inverse rotation angles of gates in \hat{U}_S . The key idea of the implemented algorithm (displayed schematically in Fig. 1a,b — see also [40–44] for related works) was to use a subset of qubits as auxiliaries, tuning their quasienergies and couplings to system qubits in order to resonantly transfer excitations from the system. The entropy of the system is removed by periodically resetting the auxiliaries. In the experiment, it was shown that the system reached a steady low-energy correlated state. Furthermore, the achieved steady states could be efficiently purified to yield high fidelities with respect to the true ground states, and it was argued that, asymptotically, the dissipative preparation is advantageous compared to variational unitary protocols.

This progress calls for the development of practical, robust, dissipative many-body state preparation algorithms. In this work, we develop a theory of quasiparticle cooling on quantum processors, concentrating on efficient preparation of phases of matter with low-energy quasiparticle excitations, in realistic noisy environments. In such many-body systems, excited states at sufficiently low energy density can be described in terms of occupation numbers of non-interacting bosonic or fermionic degrees of freedom [45]. The quasiparticles generally have a finite lifetime, due to the decay to other states; however, provided this lifetime is sufficiently long, quasiparticle description can be employed. A celebrated example is the Landau Fermi-liquid theory, which provides a description of interacting electrons in metals in terms of fermionic quasiparticles [45]. We note that quasiparticle description applies to a variety of phases of matter including Fermi liquids, superconductors, and magnetically

ordered states.

Focusing on 1d qubit – or, equivalently, spin-1/2 – systems, we consider generalised auxiliary-reset algorithms encompassing the one implemented in the experiment of Ref. [38]. We derive a dissipative kinetic equation describing the quasiparticle population dynamics under the action of the protocol, which allows for a transparent physical picture on how different parameters affect the state preparation fidelity. In particular, we investigate the effects of: (i) auxiliary layout as shown in Fig. 1c,d, with auxiliaries only at the system boundaries (edge cooling setup) or with a finite density of auxiliaries in the thermodynamic limit (bulk cooling setup); and (ii) the time dependence of the system-auxiliary couplings. We find that the latter is crucial in reaching high fidelities, and we introduce a protocol with modulated couplings to drastically reduce unwanted heating processes arising due to the finite duration of a cooling cycle. Below, we characterize the protocol performance by log-fidelity per qubit, $-\log \mathcal{F}/N_S$, where \mathcal{F} is the fidelity of the steady state with respect to the true ground state, and N_S is the number of system qubits. We argue that, if the steady state is sufficiently close to the ground state, this quantity is related to the steady-state quasiparticle density n via $-\log \mathcal{F}/N_S \approx n$. Within our kinetic equation approach, we find $n \sim \exp(-\Omega(\Delta T))$ under the modulated coupling protocol, where Δ is the quasiparticle excitation gap and T is the number of unitary layers before the auxiliaries are reset (see Fig. 1b). Thus, high fidelity can be achieved by increasing parameter T .

We assess the validity of our theory first with the example of an integrable 1d transverse-field Ising model (TFIM) spin chain, where quasiparticles are infinitely long-lived and the relevant operators are known explicitly [46, 47]. This model exhibits two phases, a paramagnetic (PM) and an antiferromagnetic (AFM) phase. The distinct nature of the quasiparticle type in the two phases (magnons in the paramagnet and domain walls in the antiferromagnet), as well as spontaneous symmetry breaking in the AFM phase, lead to qualitative differences in the importance of different cooling processes. By performing extensive numerical simulations, we show that the kinetic equation correctly captures the system’s evolution and its steady state even at a relatively strong auxiliary-system coupling — the regime relevant for current experiments. We compare the experimental protocol of Ref. [38] (where the couplings were kept constant) to our modulated coupling protocol, finding that the latter allows for much higher fidelities in the limit of large T .

Noise, inevitably present in today’s quantum simulators and processors, severely limits the performance of quantum algorithms. For example, superconducting qubits are subject to dephasing and decay processes, which introduce unwanted quasiparticles to the system. We modify the kinetic equation by incorporating noise-induced heating on top of the cooling protocol, and investigate how the non-equilibrium distribution of quasiparticle level occupations in the steady state is affected

by noise. For the Floquet TFIM example, we observe that the density n of quasiparticles in the steady state scales differently with the Markovian noise strength in the two phases. Characterizing decoherence by a dimensionless parameter γ , which reflects the noise-induced error probability per qubit over one period of Floquet evolution, we find scaling $n \propto \gamma$ in the PM phase, while in the AFM phase, we observe a crossover between linear behaviour and a scaling $n \propto \sqrt{\gamma}$. This scaling behaviour was predicted in Ref. [43], and can be understood within the kinetic framework from the nature of different quasiparticle types in the two phases. Achieving low quasiparticle densities in the AFM phase therefore requires significantly weaker noise, compared to the PM phase. Nevertheless, we find that the modulated coupling protocol achieves high fidelities when the noise rate is small compared to the auxiliary-system coupling strength.

While we largely focus on cooling in the integrable TFIM model, we expect the quasiparticle cooling algorithm to be effective also for non-integrable systems. Indeed, many such systems have low-energy quasiparticles which become weakly interacting at low energy densities. Thus, at least at low energies (the most relevant regime for ground state preparation), our analysis should apply. We illustrate the versatility of our approach by studying cooling in a TFIM with broken integrability [48], where we observe similar efficiency of our protocol as in the integrable case.

The rest of the paper is organized as follows: in Section II we describe the quasiparticle cooling protocol, and derive an equation that describes the evolution of the quasiparticle level populations, assuming a weak auxiliary-system coupling. We introduce the modulated coupling protocol (MCP) to suppress unwanted heating processes. In Section III, we turn to cooling the integrable TFIM. We analyse cooling with boundary auxiliaries and with a finite density of auxiliaries, for different cooling protocols. We find that the MCP leads to effective cooling, which can be accurately captured by the kinetic equation of Sec. II. Noise is introduced in Section IV: we examine how noise processes (dephasing and decay) affect the cooling, and show that these effects can be included into the kinetic description without complication. In Section V, we apply our protocol to study a non-integrable model, the TFIM with an additional longitudinal field. Finally, in Section VI, we provide concluding remarks and directions for future work.

II. QUASIPARTICLE COOLING PROTOCOL

A. Setup and protocol

We consider the following general setup for a system of qubits, or spins-1/2, a particular version of which was realized in the recent experiment with the Google quantum processor [38]. The central idea follows Ref. [27], and the main developments we present here

are (i) the derivation of a simplified kinetic theory, based on the quasiparticle picture, and (ii) the introduction of time-dependent system-bath coupling, which, as we will see below, is crucial to reach high fidelities.

The qubits are divided into two groups, N_S qubits forming a system of interest, and N_A auxiliary qubits acting as a bath. One cycle of the protocol (*cooling cycle*), which effectively realizes a Floquet system coupled to an engineered bath, entails the following steps:

- (i) Auxiliary qubits are initialized in a state described by a density matrix $\hat{\rho}_B^0$.
- (ii) T layers of unitary evolution are applied. A unitary applied at time step $1 \leq \tau \leq T$ is a combination of the Floquet operator \hat{U}_S acting on system qubits, a unitary \hat{U}_B acting on the bath qubits, and an interaction term $\hat{U}_{\theta,\tau}$ which couples system and bath qubits. The interaction terms is generally time-dependent, and θ is the coupling strength (see Eq. (8) below).
- (iii) The bath qubits are reset into the initial state $\hat{\rho}_B^0$, which we will assume to be a stationary state of the bath unitary \hat{U}_B .

The main protocol control parameters are T , which we refer to as the *reset time*, and the system-auxiliary coupling. Resetting auxiliary qubits at the end of the cycle defines a quantum channel acting on the system,

$$\Phi(\hat{\rho}_S) = \text{Tr}_B \hat{U}_T(\hat{\rho}_S \otimes \hat{\rho}_B^0)\hat{U}_T^\dagger, \quad (1)$$

where \hat{U}_T is the combined cooling cycle unitary,

$$\hat{U}_T = \hat{U}_{\theta,T}\hat{U}_B\hat{U}_S \dots \hat{U}_{\theta,1}\hat{U}_B\hat{U}_S, \quad (2)$$

the operator $\hat{\rho}_S$ is the system density matrix at the start of the cycle, and Tr_B is the trace over the bath degrees of freedom. The system density matrix after ν cooling cycles is given by

$$\hat{\rho}_S^\nu = \Phi^\nu(\hat{\rho}_S^0). \quad (3)$$

We will assume the steady state of the dynamics is unique, and is therefore reached independent of the initial state. In the analysis below we therefore take the initial state to be the maximally mixed state, $\hat{\rho}_S^0 \propto \hat{I}$, unless specified otherwise.

The system Floquet \hat{U}_S can in particular correspond to an exact or prethermal effective Hamiltonian \hat{H}_{eff} ,

$$\hat{U}_S \approx \exp\left(-\frac{i\pi}{2}\hat{H}_{\text{eff}}\right), \quad (4)$$

and our goal is to engineer dissipative evolution such that the steady state ($\nu \rightarrow \infty$) of the system is close to the ground state of \hat{H}_{eff} . In order to have a concrete model in mind, we will later study cooling in the case of the 1d Floquet transverse-field Ising model,

$$\hat{U}_S = \exp\left(-\frac{i\pi J}{2} \sum_{i=1}^{N_S-1} \hat{X}_i \hat{X}_{i+1}\right) \exp\left(\frac{i\pi g}{2} \sum_{i=1}^{N_S} \hat{Z}_i\right). \quad (5)$$

Here and below $\hat{X}_i, \hat{Y}_i, \hat{Z}_i$, denote the Pauli operators for qubit i , normalized as $\hat{X}_i^2 = \hat{Y}_i^2 = \hat{Z}_i^2 = 1$. The Floquet TFIM is exactly solvable via the Jordan-Wigner mapping to a model of non-interacting fermionic quasiparticles (see Appendix C), and so provides a convenient setting to study quasiparticle cooling.

We keep the bath evolution simple, assuming for the initial bath state the product state with all spins up,

$$\hat{\rho}_B^0 = \otimes_{j=1}^{N_A} |0\rangle_j \langle 0| \quad (6)$$

— note that in our convention the spin-up state is identified with the $|0\rangle$ state of the qubits — and for the bath unitary we choose

$$\hat{U}_B = \exp\left(\frac{i\pi h}{2} \sum_{j=1}^{N_A} \hat{Z}_j\right), \quad (7)$$

so that each auxiliary qubit simply acquires a phase in the eigenbasis of the \hat{Z} operator. More complicated (e.g. interacting) baths can be considered with possible advantages. Parameter πh is referred to as the *auxiliary quasienergy* and does not depend on the unitary step τ .

In contrast, the system-bath coupling will in general vary in time:

$$\hat{U}_{\theta,\tau} = \exp(-i\theta f_\tau \hat{V}), \quad \hat{V} = \sum_{j=1}^{N_A} \hat{V}_j. \quad (8)$$

We have chosen to separate the time-dependence into the function f_τ , normalised according to $\sum_{\tau=1}^T f_\tau = 1$ [49], keeping θ as a small parameter which controls the coupling strength. Both f_τ and θ are dimensionless, and the interaction operator, which has dimension of energy, can in general be written in the form

$$\hat{V} = \sum_a \hat{A}^{a\dagger} \hat{B}^a + \hat{A}^a \hat{B}^{a\dagger}, \quad (9)$$

where operators \hat{A} (\hat{B}) acts on system (bath). Note that index a does not have to be identical to the index numbering auxiliary qubits.

A particular form of interaction that we will consider below arises when an auxiliary \mathcal{A}_j is coupled to a single qubit \mathcal{Q}_j of the system by an operator \hat{V} that can generate a partial iSWAP gate:

$$\hat{V} = \pi \sum_j (\hat{\sigma}_{\mathcal{Q}_j}^+ \hat{\sigma}_{\mathcal{A}_j}^- + \hat{\sigma}_{\mathcal{Q}_j}^- \hat{\sigma}_{\mathcal{A}_j}^+), \quad (10)$$

At weak coupling, the occupation number change over one cycle, $\delta n_k = n'_k - n_k$, is small, and we compute it by expanding the r.-h.s. of the above equation to the second order in θ . Noting that the linear order in θ vanishes, and defining

$$\delta n_k = \text{Tr}_S(\hat{\rho}_S \delta \hat{n}_k), \quad \delta \hat{n}_k = \text{Tr}_B\left(\hat{\rho}_B^0 \left[\hat{U}_T^\dagger \hat{n}_k \hat{U}_T\right]\right) - \hat{n}_k, \quad (15)$$

where \mathcal{Q}_j (\mathcal{A}_j) represent system (auxiliary) position associated with j -th coupling. Here $\hat{\sigma}^\pm = \frac{1}{2}(\hat{X} \pm i\hat{Y})$ are spin raising/lowering operators.

B. Weak-coupling analysis

In the remaining theoretical analysis, we assume that the excitations of the many-body system are well-defined, long-lived quasiparticles, and that we are in the limit of weak system-bath coupling, $\theta|V_j| \ll 1$. The quasiparticle assumption holds exactly in the example of the TFIM, Eq. (5); we note, however, that interacting systems away from criticality typically have quasiparticle excitations – examples include Fermi-liquids, superconductors, and symmetry-broken magnetic phases [45]. We expect the quasiparticle cooling algorithm to remain effective for such interacting systems. Our strategy will be to derive an equation describing evolution of the quasiparticle level occupations in the weak-coupling limit.

We define the quasiparticle occupation number operator \hat{n}_k , where index k labels fermionic quasiparticle levels (e.g. momentum in a system with periodic boundary conditions). The quasiparticles are sufficiently long-lived, such that \hat{n}_k is an integral of motion of the system's evolution operator,

$$\hat{n}_k \hat{U}_S = \hat{U}_S \hat{n}_k. \quad (11)$$

In practice, it is sufficient to assume that the quasiparticle lifetime is much longer than the duration of one cooling cycle.

It is convenient to work in the interaction picture with respect to the evolution operator $\hat{U}_0 = \hat{U}_B \hat{U}_S$, such that an operator \hat{O}_τ (originally in the Schrödinger picture) is given by:

$$\hat{O}_{I\tau} = \hat{U}_0^{-\tau} \hat{O}_\tau \hat{U}_0^\tau, \quad 1 \leq \tau \leq T. \quad (12)$$

The evolution operator can be rewritten as follows,

$$\hat{U}_T = \hat{U}_0^T \hat{U}_T, \quad \hat{U}_T = \mathcal{T} \exp\left(-i\theta \sum_{\tau=1}^T f_\tau \hat{V}_{I\tau}\right), \quad (13)$$

where \mathcal{T} denotes time-ordering. Taking into account Eqs. (1,11), the quasiparticle occupation number after one cooling cycle reads:

$$n'_k = \text{Tr}_S(\Phi(\hat{\rho}_S) \hat{n}_k) = \text{Tr}_{SB}\left(\hat{\rho}_S \otimes \hat{\rho}_B^0 \left[\hat{U}_T^\dagger \hat{n}_k \hat{U}_T\right]\right), \quad (14)$$

this yields:

$$\delta\hat{n}_k = \theta^2 \sum_{ab} \sum_{\tau_1=1}^T \sum_{\tau_2=1}^T f_{\tau_1} f_{\tau_2} \Gamma_{ab}(\tau_1 - \tau_2) \left(\hat{A}_{I\tau_1}^{a\dagger} \hat{n}_k \hat{A}_{I\tau_2}^b - \frac{1}{2} \{ \hat{n}_k, \hat{A}_{I\tau_1}^{a\dagger} \hat{A}_{I\tau_2}^b \} \right) + i\theta^2 [\hat{H}_{\text{LS}}, \hat{n}_k]. \quad (16)$$

Here we defined the autocorrelators of the \hat{B} operators,

$$\Gamma_{ab}(\tau) = \text{Tr}_B \left(\hat{\rho}_B^0 \hat{B}_{I\tau}^{a\dagger} \hat{B}_{I0}^b \right), \quad (17)$$

and used relations $\Gamma_{ab}(\tau) = \Gamma_{ba}^*(-\tau)$. The second term in the r.h.s. of Eq. (16) can be viewed as arising from the ‘‘Lamb shift’’ renormalization:

$$\hat{H}_{\text{LS}} = \frac{i}{2} \sum_{ab} \sum_{\tau_1=1}^T \sum_{\tau_2=1}^T f_{\tau_1} f_{\tau_2} (\Theta(\tau_1 - \tau_2) - \Theta(\tau_2 - \tau_1)) \Gamma_{ab}(\tau_1 - \tau_2) \hat{A}_{I\tau_1}^{a\dagger} \hat{A}_{I\tau_2}^b. \quad (18)$$

where $\Theta(\tau)$ is the standard Heaviside step function, with the convention $\Theta(0) = 1/2$.

C. Rate equation

Note that the above derivation so far follows the steps of the textbook derivation of the Lindblad equation [50, 51], except here we focus on the Heisenberg-picture evolution of the occupation number operators, rather than on the system’s density matrix. However, to derive the Lindblad equation one typically assumes a rapid decay of bath temporal correlations, compared to system’s dynamical timescales; in contrast, in our analysis the memory effects of the bath will play an essential role.

To simplify the analysis, we make an assumption that the system’s density matrix in the beginning of a cooling cycle is diagonal in the quasiparticle basis, $[\hat{\rho}_S, \hat{n}_k] = 0$. Moreover, we will make a further assumption that the correlations between occupations of different levels can be neglected (closely related to molecular chaos assumption in kinetic theory). The former assumption can be justified in the limit $\theta \rightarrow 0$, by coarse-graining over sufficiently many cooling cycles (secular approximation). The latter assumption is more difficult to prove [52]. However, as we will show below, these assumptions lead to a theory of quasiparticle cooling which is in quantitative agreement with numerical simulations.

Under these two assumptions, the system’s density matrix is given by $\hat{\rho}_S = \sum_{\vec{\alpha}} \rho_{\vec{\alpha}\vec{\alpha}} |\vec{\alpha}\rangle \langle \vec{\alpha}|$, where $|\vec{\alpha}\rangle$ form a basis of states with occupation numbers $\{\alpha_k\}$, $\alpha_k = 0, 1$

and quasienergy

$$\varepsilon(\vec{\alpha}) = \sum_k \epsilon_k \alpha_k,$$

where ϵ_k is quasienergy of quasiparticle level k . The probability $\rho_{\vec{\alpha}\vec{\alpha}}$ can be expressed in terms of *average* occupation numbers $n_q = \text{Tr}(\hat{\rho}_S \hat{n}_q)$ via

$$\rho_{\vec{\alpha}\vec{\alpha}} = \prod_q n_q^{\alpha_q} (1 - n_q)^{1 - \alpha_q}. \quad (19)$$

Note that in writing this form, we used the assumption that there are no correlations between occupations of different quasiparticle states. This ansatz can also be viewed as a time-dependent Generalized Gibbs ensemble (GGE) ansatz for $\hat{\rho}$ [53, 54].

Next, we compute the change in the occupation number over one cycle, δn_k using the above form of the density matrix and Eq. (16). Since density \hat{n}_k commutes with $\hat{\rho}_S$, the Lamb shift contribution plays no role. Denoting the Bohr frequencies by

$$\Delta(\vec{\alpha}, \vec{\beta}) = \varepsilon(\vec{\alpha}) - \varepsilon(\vec{\beta}), \quad (20)$$

we obtain

$$\delta n_k = \theta^2 \sum_{\vec{\alpha}, \vec{\beta}} \sum_{a,b,\tau_1,\tau_2} \rho_{\vec{\alpha}\vec{\alpha}} (\beta_k - \alpha_k) f_{\tau_1} f_{\tau_2} \Gamma_{ab}(\tau_1 - \tau_2) e^{i(\tau_1 - \tau_2) \Delta(\vec{\alpha}, \vec{\beta})} \langle \vec{\alpha} | \hat{A}^{a\dagger} | \vec{\beta} \rangle \langle \vec{\beta} | \hat{A}^b | \vec{\alpha} \rangle \quad (21)$$

This equation illustrates that the quasiparticle number evolution is controlled by (i) spectral correlations of the bath, given by $\Gamma_{ab}(\tau_1 - \tau_2)$, (ii) the choice of the time-dependent coupling, f_τ , and (iii) the matrix elements

of the operators \hat{A}^a entering auxiliary-system coupling. With our above choice of bath unitary (7) and coupling

(10), the bath spectral function reads

$$\Gamma_{\mathcal{A}_j \mathcal{A}_l}(\tau) = \langle \vec{0} | \hat{\sigma}_{\mathcal{A}_j}^-(\tau) \hat{\sigma}_{\mathcal{A}_l}^+(0) | \vec{0} \rangle = \delta_{jl} e^{-i\pi h \tau}, \quad (22)$$

and Eq. (21) takes the following form:

$$\delta n_k = \theta^2 \sum_{j=1}^{N_A} \sum_{\vec{\alpha}\vec{\beta}} \rho_{\vec{\alpha}\vec{\beta}}(\beta_k - \alpha_k) |F_{h,T}(\Delta(\vec{\alpha}, \vec{\beta}))|^2 |\langle \vec{\beta} | \hat{\sigma}_{\mathcal{Q}_j}^+ | \vec{\alpha} \rangle|^2. \quad (23)$$

where

$$F_{h,T}(\epsilon) = \pi \sum_{\tau=1}^T f_{\tau} e^{i\tau(\epsilon - \pi h)}. \quad (24)$$

We refer to $F_{h,T}(\epsilon)$ as the *filter function* associated with f_{τ} , essentially being its Fourier transform. Eq. (23) is a general rate equation for quasiparticle level occupation numbers. Next, we discuss how the auxiliary quasienergy πh and the coupling f_{τ} can be tailored to remove quasiparticles from the system, driving it towards the ground state.

D. Two cooling protocols

In Eq. (23) above we expressed the change in the occupation numbers in terms of the transition rates between many-body states $|\vec{\alpha}\rangle$ and $|\vec{\beta}\rangle$ induced by the coupling to auxiliaries. It is natural to consider the prethermal limit where quasiparticle quasienergies are close to the energies of quasiparticles of the corresponding prethermal Hamiltonian [39]. For example, transverse-field Ising model with arbitrary integrability-breaking local terms is in the prethermal regime as long as $|J|, |g| \ll 1$ and a similar condition is satisfied by the additional, integrability-breaking terms. In the prethermal regime, generally $|\epsilon_k| \ll \pi$. We note that in this limit, the heating processes due to Floquet evolution, and the associated energy non-conservation, are suppressed exponentially in $1/|g|, 1/|J|$.

The above rate equation (23) includes both heating ($\Delta(\vec{\alpha}, \vec{\beta}) < 0$) and cooling ($\Delta(\vec{\alpha}, \vec{\beta}) > 0$) processes. To ensure effective cooling, the filter function should be engineered to satisfy (for $\epsilon > 0$):

$$\left| \frac{F_{h,T}(+\epsilon)}{F_{h,T}(-\epsilon)} \right| \gg 1. \quad (25)$$

The prethermalization assumption allows us to neglect processes where quasienergy changes by $\pm 2\pi, \pm 4\pi$ etc, since the corresponding matrix elements are strongly suppressed. Below, we will introduce two protocols that realize Eq. (25) to different degrees.

1. Step-wise cooling protocol (SCP)

In the first strategy, one aims to resonantly remove single quasiparticles from the system, by approximately matching auxiliary excitation quasienergy πh to a value ϵ within the quasiparticle band, $\Delta < \epsilon < \Delta + W$, where Δ is the single-particle quasienergy gap and W is the bandwidth. The function

$$f_{\tau} = 1/T \quad (26)$$

is kept constant, therefore giving a ‘step’ pulse for $1 \leq \tau \leq T$. We will refer to this approach as the *step-wise cooling protocol (SCP)*.

We note that the SCP is the strategy used in Ref. [38]. The filter function corresponding to the SCP gives, up to a phase factor,

$$F_{h,T}^{\text{SCP}}(\epsilon) = \frac{\pi \sin[(\epsilon - \pi h)T/2]}{T \sin[(\epsilon - \pi h)/2]}, \quad (27)$$

which for $T \gg 1$ has a sharp peak at $\epsilon = \pi h$, with a width of order $\delta\epsilon = \frac{2\pi}{T}$. Thus, in the SCP, the processes of quasiparticle removal with quasienergies $\epsilon \approx \pi h$ are favored approximately according to

$$\left| \frac{F_{h,T}^{\text{SCP}}(+\pi h)}{F_{h,T}^{\text{SCP}}(-\pi h)} \right| \approx hT. \quad (28)$$

The SCP is efficient in systems with a sufficiently large quasiparticle gap, as demonstrated in [38]. However, as the gap is decreased, in particular when a quantum critical point is approached, the heating processes become more important. Even in a gapped phase, the suppression of heating is only algebraic in quasiparticle energy, which leads to non-zero quasiparticle density in the steady state. Therefore, SCP does not allow to prepare a many-body ground state with high fidelity.

2. Modulated cooling protocol (MCP)

Alternatively, the coupling strength f_τ can be modulated in time such that $F_{h,T}(\epsilon)$ leads to approximately exponential suppression of heating transitions. One particular choice of f_τ is

$$f_\tau = \frac{1}{A\beta} \frac{\sin[\pi(\tau - \tau_0)/2]}{\sinh[\pi(\tau - \tau_0)/\beta]}, \quad (29)$$

where $\tau_0 = T/2$, A is the normalization factor [55]. The auxiliary quasienergy is fixed at $\pi h = \pi/2$. We call this approach the *modulated cooling protocol (MCP)*.

In the SCP, transitions occur at the natural resonant frequency of the auxiliary qubits; in the MCP, the resonant frequencies are engineered according to modulation in the time-domain. More specifically, the MCP is designed to satisfy the thermal detailed balance condition, and $F_{h,T}$ takes the form of a broadened step-function (Fermi distribution) in frequency space for $1 \ll \beta \ll T$, with ‘thermal’ broadening $\sim 1/\beta$:

$$F_{h,T}^{\text{MCP}} \approx \pi \left[\frac{\tanh(\epsilon\beta/2) - \tanh((\epsilon - \pi)\beta/2)}{\tanh(\pi\beta/4)} \right]. \quad (30)$$

We refer the reader to Appendix A for the derivation of this formula in the limit where $T \rightarrow \infty$, and $0 < \beta/T \ll 1$, and Appendix B for a more detailed discussion of the detailed balance condition. The frequency-step form of the MCP leads to a suppression

$$\left| \frac{F_{h,T}^{\text{MCP}}(+\epsilon)}{F_{h,T}^{\text{MCP}}(-\epsilon)} \right| \approx e^{\epsilon\beta}, \quad (31)$$

and heating transitions are now *exponentially* suppressed. We have also verified that the step-like form of $F_{h,T}^{\text{MCP}}(\epsilon)$ is realized for moderate values of $T \approx 10$, which is the practical regime in the presence of noise.

In the rest of this paper, we focus on cooling *gapped* quasiparticle systems, with $\Delta > 0$. As in the case of thermal equilibrium, we anticipate the difficulty of cooling gapless systems to their ground state, since zero energy modes may be excited by arbitrarily small heating elements for any finite β (in the case of the MCP). Indeed, on general grounds of the energy-time uncertainty relation, we expect modes of energy ϵ require times $T \approx \epsilon^{-1}$ to cool.

We note that other, more general protocols can be constructed, which in certain cases may improve cooling efficiency. In particular, h can be modulated during the cooling cycle, as in the adiabatic demagnetization protocol recently studied in Ref. [43]. In Sec. V, when considering cooling of non-integrable systems, we will also vary the coupling strength θ over cooling cycles in order to reach the steady state more rapidly. Our intention

with introducing the two protocols above is to provide a basis for effective cooling, and in particular to highlight the role of modulating the coupling pulse to block unwanted heating.

III. THEORY OF QUASIPARTICLE COOLING IN A SPIN CHAIN

In this Section, we study the performance of the cooling algorithms using the example of the TFIM, specified by the Floquet operator in Eq. (5). We assume the absence of noise (which we include in Section IV). We first consider the edge auxiliary setup (Fig. 1c). We will see that this leads to solvable dynamics in the sense that the density matrix of the system remains Gaussian. We show that the predictions of the rate equation derived above are in excellent agreement with the exact numerical solution. Further, we study the bulk auxiliary setup (Fig. 1d), where integrability is broken by the coupling to auxiliaries. In this case we compare the rate equation predictions to matrix-product states simulations of the dissipative evolution, finding again a good agreement. We investigate the dominant cooling and heating processes in the two phases, paramagnetic (PM) and antiferromagnetic (AFM), of the TFIM, finding qualitative differences due to the different nature of quasiparticles. By comparing the performance of the SCP and MCP, we find that the latter allows ground state preparation with a fidelity arbitrarily close to 1, in the noiseless case, by increasing the parameter β .

A. Transverse-field Ising model

We start by briefly summarizing the properties of the Floquet TFIM. This model can be mapped onto a p -wave superconducting chain by the Jordan-Wigner transformation:

$$\hat{\sigma}_j^- = \prod_{i=1}^{j-1} e^{i\pi\hat{c}_i^\dagger\hat{c}_i} \hat{c}_j^\dagger, \quad \hat{Z}_j = 1 - 2\hat{c}_j^\dagger\hat{c}_j, \quad (32)$$

where $\hat{c}_j^\dagger, \hat{c}_j$ are fermionic creation/annihilation operators. The quasiparticle bands have quasienergies ϵ_k given by:

$$\cos \epsilon_k = \cos(\pi J) \cos(\pi g) - \sin(\pi J) \sin(\pi g) \cos k, \quad (33)$$

where $k \in [-\pi; \pi]$ is a quasimomentum. As a function of parameters J and g , the model has four phases, separated by phase transition lines at $J = g$, $J = 1 - g$, where the quasiparticle gap Δ closes. The four phases are distinguished by the 0 and π Majorana edge modes [56–58]. Here we will be interested in the part of the phase diagram where $0 < J, g < 1/2$, and two phases exist: a paramagnetic (PM) phase at $g > J$, and an antiferromagnetic (AFM) phase at $g < J$. For $g, J \rightarrow 0$ these are

the phases of the Hamiltonian TFIM; by analogy to this case, we define the Floquet vacuum projector

$$\Omega = \sum_g |\Omega_g\rangle\langle\Omega_g| \quad (34)$$

to project onto states where the valence quasiparticle band is filled, and the conduction band is empty i.e. $\hat{c}_k|\Omega_g\rangle = 0, \forall k$. The index g runs over the possible ground states: in the PM phase the vacuum state is unique, while in the AFM phase in the limit $N_S \rightarrow \infty$, the vacuum state is doubly degenerate, $g = \pm 1$, and the \mathbb{Z}_2 symmetry is spontaneously broken. In the fermionic counterpart of the TFIM, this degeneracy stems from the existence of zero-(quasi)energy Majorana edge modes, and the two vacuum states of the AFM differ by occupation of the Majorana level. The quasienergy gap between the ground and first excited state is given by $\Delta = 2\pi|J - g|$. In the rest of the paper, unless otherwise stated, results for the AFM (PM) phase correspond to the parameter points $J = 0.2$ (0.1), $g = 0.1$ (0.2).

For the open-boundary chain we consider, the allowed quasimomenta are quantized, $k_m \approx \pi(m - 1)/N_S$, $m = 1, 2, \dots, N_S$, and the fermionic eigenmodes, defined by creation/annihilation operators $\hat{\eta}_k^\dagger, \hat{\eta}_k$, are superpositions of plane waves with wave-vectors $\pm k$ (standing waves). The relation between on-site fermionic operators and eigenmodes is

$$c_j = \sum_k u_{jk}\eta_k + v_{jk}\eta_k^\dagger, \quad (35)$$

with the coefficients u, v referred to as the ‘Bogoliubov coefficients’. We refer to Appendix C for a more detailed discussion and explicit relations.

B. A solvable model: cooling at the edge

We now study a solvable example of cooling in the edge auxiliary setup of Fig 1c. In this case, the auxiliary coupling operator $\hat{\sigma}_1^\pm$ is free of the Jordan-Wigner string in the fermionic language, being proportional to c_1^\dagger, c_1 (see Eq. (32)). Therefore, in the rate equation (23), only processes where occupation of one of the quasiparticle levels changes by ± 1 are allowed. Due to reflection symmetry, the auxiliary at the other edge contributes equally to the cooling process, and after some algebra, Eq. (23) takes the form:

$$\delta n_k = -n_k W_k^- + (1 - n_k) W_k^+, \quad (36)$$

with the single-particle cooling and heating rates

$$W_k^- = 2\theta^2 |F_{h,T}(+\epsilon_k)|^2 |u_{1k}|^2, \quad (37)$$

$$W_k^+ = 2\theta^2 |F_{h,T}(-\epsilon_k)|^2 |v_{1k}|^2. \quad (38)$$

The coefficients $|u_{1k}|^2, |v_{1k}|^2$ naturally represent the probabilities for the quasiparticle (quasihole) to be found

at the boundary. Assuming that the system is away from the critical point, the probabilities scale as $O(N_S^{-1})$ (from the normalization condition) away from the band edge, but are $O(k^2 N_S^{-1}) \approx O(N_S^{-3})$ near the band edge $k \approx 0, \pi$. This leads to a pronounced dependence of the cooling rates on the quasienergy ϵ_k , with the late time dynamics dominated by the cooling of modes near the band edges. Eq. (36) can be solved for the steady state populations

$$n_k^\infty = \frac{W_k^+}{W_k^+ + W_k^-}, \quad (39)$$

showing that a finite heating rate will inevitably lead to non-zero quasiparticle population.

We will compare the rate equation predictions to exact numerical simulations, which can be performed efficiently in the case of edge cooling: due to the free-fermion nature of the TFIM with boundary auxiliaries, Eq. (1) defines a Gaussian channel, so starting from an initial Gaussian state, such as the identity state, Wick’s theorem guarantees that the complete many-body state information is captured by the $2N \times 2N$ -dimensional matrix of 2-point fermion correlators, where $N = N_S + 2$ is the number of system qubits plus the two auxiliaries. By numerical evolution of the correlation matrix we can assess the accuracy of the rate equation in capturing the two protocols. Further detail on the numerical steps is provided in Appendix E.

As a first characterisation of the cooling performance, we study the dynamics of the quasiparticle density $n(t) = N_S^{-1} \sum_k n_k(t)$. In Fig. 2a,b we plot $n(t)$ for both protocols, SCP and MCP, in the two phases, starting from the maximally mixed state $n(0) = 1/2$. We take $T = 4, h = 0.3$ in the SCP, and $T = 28 = 3\beta, h = 0.5$ in the MCP; the smaller reset time in the SCP case is approximately optimal (see Fig. 2c) while the MCP choice corresponds to $\beta \approx 2\pi\Delta^{-1}$. In both cases $\theta = 0.02$ and $N_S = 20$. We observe a very good agreement between the rate equation theory (dashed lines) and the exact numerical simulation (solid lines). In the considered time window, for both PM and AFM phases under the MCP, the density decays predominantly exponentially in time, with a rate proportional to θ^2 . In accordance with the arguments regarding heating rates in Section II, the MCP exhibits a saturation of $n(t)$ at a much smaller value than the SCP (though in that case, the saturation is still to a relatively small value on account of the large quasiparticle gap). We also note the long time-scales associated with cooling to states of low quasiparticle density, with $\nu \approx 300\theta^{-2}$ for the PM phase under the MCP and even greater for the AFM. This is a consequence of the edge cooling setup, and the scaling of the Bogoliubov coefficients near the band edge discussed above.

As a second test, we examine the fidelity of the steady state distribution with respect to the Floquet vacuum, $\mathcal{F} = \text{Tr}(\Omega\rho)$. In the case where Eq. (19) holds, the fidelity

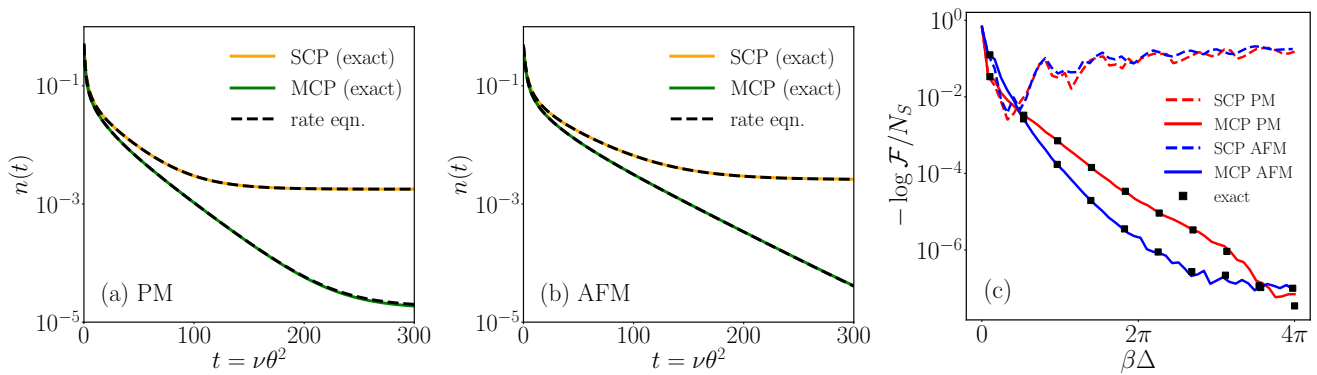


Figure 2. Performance of edge cooling protocol, for the parameter choice described in the main text. (a) Evolution of quasiparticle density $n(t)$ as a function of rescaled timescale $t = \nu\theta^2$, where ν is total number of cooling cycles, for the PM phase. We compare exact numerical results with $\theta = 0.02$ (solid lines) and the rate equation (dashed lines), for both SCP and MCP. (b) Same as in (a) but for AFM phase; (c) Log-fidelity per qubit of the steady state with quasiparticle vacuum, obtain from kinetic equation, as a function of the MCP parameter $T = 3\beta$. Black squares are exact numerical data, with $\theta = 0.001$, showing that kinetic theory accurately captures the steady-state properties.

can be rewritten

$$\mathcal{F} = \prod_k (1 - n_k) \approx \exp\left(-\sum_k n_k\right). \quad (40)$$

The second line holds in the limit of sufficiently low total quasiparticle density. In this regime, the log-fidelity per qubit and quasiparticle density are approximately synonymous. In Fig. 2c we plot the steady state fidelity for the two pulses as the parameter β is increased, with $T = 3\beta$ fixed (for the SCP this is just a variation of parameter T). For parameters considered, the SCP allows to reach fidelity of order 0.99 per qubit while the MCP fidelity (per qubit) is better than one part in 10^6 by the point $\beta\Delta \approx 4\pi$. From Eq. (31), we see that the density of quasiparticles is bounded approximately as $n \sim e^{-\beta\Delta}$. The apparent saturation of MCP around $\beta\Delta = 4\pi$ is due to small ringing errors, which can be removed by increasing the ratio T/β — we refer the reader to Appendix A for more details. In practice, dominant heating processes arise due to noise (see Sec. IV) and it pays to keep the ratio $T/\beta \gtrsim O(1)$.

From the above results, we conclude that the MCP is able to successfully prepare the ground state of the TFIM, with fidelity approaching 1 in the limit of large β . However, the associated time scale diverges with the system size, naturally a weakness of the edge cooling setup. The rate equation accurately captures the quasiparticle dynamics for the case of edge cooling. Next, we will consider the bulk cooling setup with a finite density of auxiliaries.

C. Finite density of auxiliaries

While providing an instructive example, the edge cooling setup is not practical for large systems. We argued above that the cooling timescale diverges with the system size in that case, which holds generally for models with local boundary dissipation [59]. Furthermore, the cooling rate remains constant while the heating rate due to noise scales with system size (see the following Section). Therefore, we now consider the setup in Fig. 1d, with a finite density of auxiliaries. For simplicity, we will assume that there is one auxiliary per system qubit.

In this setup, the dynamics is no longer integrable, and the system's density matrix develops non-Gaussian correlations due to the fact that the matrix elements for bulk σ_j^\pm operators carry Jordan-Wigner strings in the fermionic formulation (see Eq. (32)). This allows for transitions between many-body eigenstates where the occupation numbers of several quasiparticle levels change at once.

To make progress, we therefore assume that the processes involving a small number quasiparticles are dominant. For cooling processes, this assumption is justified in the low-density limit $n_k \ll 1$, which describes the system's dynamics close to the ground state [60]. Restricting to processes involving at most two quasiparticles, we derive the following kinetic equation, containing cooling and heating terms, as well as terms that describe scattering between quasiparticles:

$$\delta n_k = -n_k W_k^- + (1 - n_k) W_k^+ + \sum_q \left[-n_k W_{k,q}^- n_q + (1 - n_k) W_{k,q}^+ (1 - n_q) - n_k V_{k,q}^- (1 - n_q) + (1 - n_k) V_{k,q}^+ n_q \right]. \quad (41)$$

We compute the rates in Eq. (41) assuming the system

is near the vacuum state Ω , which yields:

$$W_k^\mp = \theta^2 \sum_{j=1}^{N_S} |F_{h,T}(\pm\epsilon_k)|^2 |\sigma_{j;0;k}^\pm|^2, \quad (42)$$

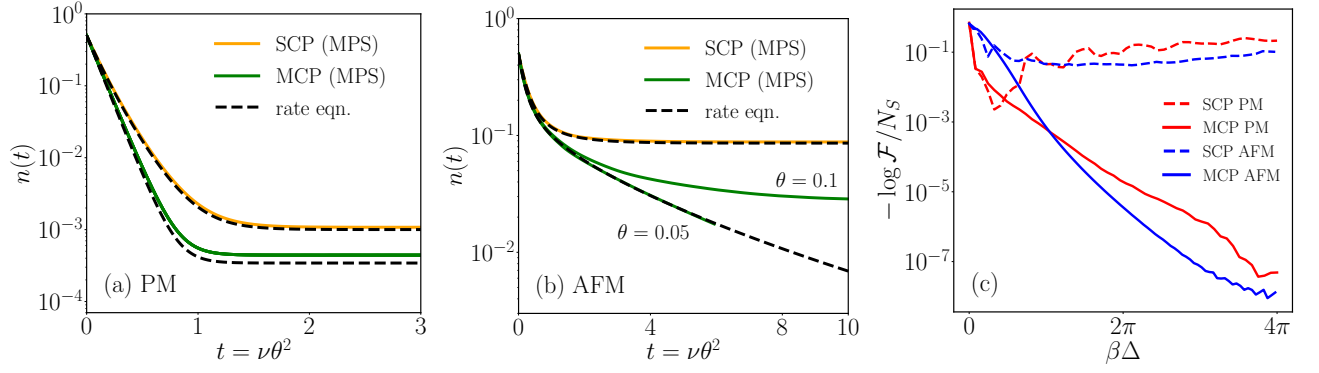


Figure 3. Performance of the bulk cooling protocol, with one auxiliary per system qubit and $N_S = 20$. The parameter choice is described in the main text. (a) Quasiparticle density $n(t)$ vs. rescaled timescale $t = \nu\theta^2$ in the PM phase. The MPS results (solid lines) are compared to the kinetic theory predictions (dashed lines), for both SCP and MCP. Parameter $\theta = 0.1$. (b) Same as in (a) but for the AFM phase. We show MPS results for two coupling strengths, $\theta = 0.1$ and 0.05 , with the larger showing corrections to the rate equation. The AFM cools more slowly than the PM, as expected due to the topological nature of the quasiparticles. (c) Log-fidelity per qubit of the steady state with quasiparticle vacuum, calculated from the kinetic equation, as a function of parameter β , related to the number of unitary layers in one cooling cycle, via $T = 5\beta$.

$$W_{k,q}^{\mp} = \theta^2 \sum_{j=1}^{N_S} |F_{h,T}(\pm(\epsilon_k + \epsilon_q))|^2 |\sigma_{j;0;k,q}^{\pm}|^2, \quad (43)$$

$$V_{k,q}^{\mp} = \theta^2 \sum_{j=1}^{N_S} |F_{h,T}(\pm(\epsilon_k - \epsilon_q))|^2 |\sigma_{j;q;k}^{\pm}|^2, \quad (44)$$

where we introduced the shorthand matrix-elements

$$\sigma_{j;k_1,\dots,k_m;k_1,\dots,k_n}^{\pm} = \langle k_1, \dots, k_m | \hat{\sigma}_j^{\pm} | k_1, \dots, k_n \rangle. \quad (45)$$

Above, the terms W_k^{\mp} correspond to cooling/heating processes involving one quasiparticle, while the terms $W_{k,q}^{\mp}$ describe removing/adding a pair of quasiparticles, and $V_{k,q}^{\mp}$ describe quasiparticle scattering. Note that while the scattering does not directly change the total quasiparticle occupation number, it will tend to move quasiparticles toward lower quasienergies due to the presence of the filter function $F_{h,T}$. We expect that these rates will be weakly affected by a small finite background density of quasiparticles. The matrix elements can be evaluated using Wick's theorem (see Appendix D and a review [61]).

Crucially, the matrix elements entering in the above rates obey different selection rules in the PM and AFM phases. In the PM phase, there is a unique symmetric ground state. Operators $\hat{\sigma}_j^{\pm}$ anticommute with the parity operator $\prod_j \hat{Z}_j$, so in the fermionic language they must change the fermion parity. Thus, two particle processes are forbidden in the PM phase, $W_{k,q}^{\mp} = V_{k,q}^{\mp} = 0$. In contrast, in the AFM phase, there are two vacuum states, $|\Omega_{\pm}\rangle$, which have parity ± 1 . The cooling process can induce transitions between them by changing the occupation of the Majorana edge fermion. $W_{k,q}^{\mp}$ and $V_{k,q}^{\mp}$ matrix elements are non-vanishing in this case. The bra and ket states should be understood as quasiparticle states on top of different vacua. Note that the Majorana edge mode

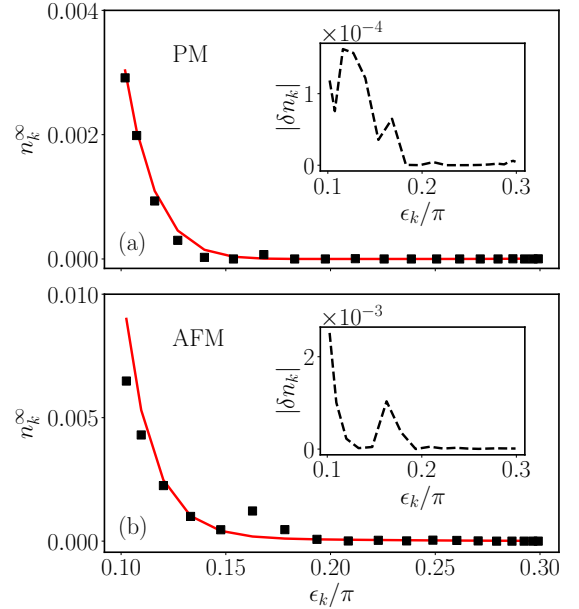


Figure 4. Quasiparticle occupation numbers n_k^{∞} in the steady state, as a function of quasienergy ϵ_k . We compare MPS simulations (scatter points) and kinetic equation results (red line), for a system with $N_S = N_A = 20$ qubits in (a) PM and (b) AFM phases. The reset time is $T = 12 = 2\beta$, and the coupling $\theta = 0.05$. The MPS simulations use a maximum bond dimension of $d = 100$. Inset: deviation $|\delta n_k|$ between rate equation and MPS values shown in main figure.

has a vanishing energy in the limit of large system size; hence, this mode cannot be cooled by our protocol and will remain effectively at an infinite temperature, corresponding to an equal weight mixture of the two vacuum states.

In the spin language, these selection rules follow from

intuitive arguments given in Ref. [43]. The quasiparticles of the PM phase are magnons, local excitations that can be removed via local spin flips (caused by auxiliary qubit interactions); in contrast, in the AFM phase, quasiparticles are domain-wall-like and can only be removed/created locally in pairs. In Appendix D, we study the distinct behavior of matrix elements in the two phases in detail. In particular, the two-particle matrix elements in the AFM phase are homogeneous in the bulk, but single-particle matrix elements decay exponentially with the distance of the auxiliary qubit from the boundary (since single domain walls can be removed at the edges of the chain), with a decay length set by the correlation length of the model. We will see below that this difference in quasiparticle nature leads to different efficiencies of the cooling in the two phases.

We now compare the predictions of the above kinetic theory to matrix product state (MPS) simulations of the system's density operator dynamics (more precisely, density matrix product operator simulations [62, 63]). The dynamics are performed using the standard time-evolving block decimation (TEBD) algorithm [64, 65], implemented via the ITensor library [66]. Implementation details and numerical verifications of asymptotic convergence are presented in Appendix E.

As illustrated in Fig. 3a,b, the theory continues to be accurate for cooling with a finite density of auxiliaries, for both the SCP and MCP protocols. We fix system size $N_S = 20$ with one auxiliary per site. We use cooling parameters $T = 5$, $h = 0.3$ in the SCP and $T = 12 = 2\beta$ in the MCP. The coupling is chosen to be $\theta = 0.1$ in the PM phase. In the AFM phase, this relatively large coupling leads to visible deviations between the MPS results and the kinetic equation prediction at late times; hence we include simulation results for a weaker coupling, $\theta = 0.05$, which leads to a good agreement. We use bond dimension $d = 100$ for both the SCP and MCP ($\theta = 0.05$) data, and $d = 150$ for the MCP ($\theta = 0.1$) data. These choices are converged in bond dimension (see Appendix E). Our choice of larger θ and smaller MCP reset time (compared to the edge cooling case) helps to avoid high entanglement at intermediate times, which affects the accuracy of the MPS simulations. The MCP outperforms the SCP, and in Fig. 3c we provide further confirmation that the MCP can reach much higher fidelities, plotting the increase in the log-fidelity per qubit as the parameter $T = 5\beta$ is increased (we choose a large value of T/β to remove the ringing artifacts for the range of fidelities shown, see Appendix A).

The difference in cooling distinct quasiparticle types in the PM and AFM phases is also evident in the timescales shown in Fig. 3a,b: the PM reaches a quasiparticle density below 10^{-3} after a small number of cooling cycles $O(\theta^{-2})$, with a clear exponential decay to the steady state value. In contrast, in the AFM phase, cooling slows down once quasiparticle density is below $n(t) \lesssim 10^{-1}$. This separation of timescales in the AFM is due to the fact that initial cooling proceeds quickly through pair

annihilation processes, but this mechanism is suppressed $\propto n^2$ in the low density regime. Late-time cooling is therefore dominated by single-particle processes, which may only occur around the system edge.

As a final comparison between the kinetic equation and the MPS numerics, we look at the momentum-resolved quasiparticle occupations in the steady state, in Fig. 4, focusing on the MCP. To reach the steady state in our MPS simulations, we perform the simulations starting from the exact ground state. As we expect the (unique) steady state to be close to the true ground state, this allows for faster real-time simulations compared to starting from a high energy-density state. The figure illustrates that occupation numbers of all levels are below 10^{-2} , and the remaining population is mostly due to quasiparticles at the band edge. The finite weight on low energy modes stems from the relatively small value of the parameter $\beta \approx 1.2\pi\Delta^{-1}$ chosen to aid the convergence of the MPS simulations.

To sum up, the analysis above demonstrates efficiency of MCP with a finite density of auxiliaries for removing quasiparticles after $O(\theta^{-2})$ cooling cycles, in the PM phase. In agreement with the arguments of Ref. [43], we also find that topological, domain-wall type quasiparticles are more challenging to remove. Nevertheless, in an idealized system without noise, our cooling protocol allows preparation of the ground state with fidelity arbitrarily close to 1.

IV. NOISE EFFECTS

Having established that the quasiparticle cooling algorithm can be used to efficiently prepare correlated ground states, we now turn to the effects of unwanted decoherence. Each experimental platform comes with its own sources of noise, and our goal will be to understand the limitations it imposes on the cooling efficiency. We will focus on the single-qubit decay and dephasing processes, relevant in systems of superconducting qubits. The kinetic equation can be generalized to include transitions mediated by weak noise. Using this modified kinetic theory, we analyze the dependence of the steady state quasiparticle population on the noise strength.

A. Rate equation in the presence of noise

Considering continuous time evolution, single-qubit decoherence processes can be conveniently described within Lindblad formalism [50]. The evolution of the system's density matrix ρ_S is given by (for the moment, we ignore presence of auxiliary qubits):

$$\begin{aligned} \frac{d\hat{\rho}_S}{dt} &= -i[\hat{H}, \hat{\rho}_S] + \delta\mathcal{D}(\hat{\rho}_S; \tilde{\gamma}), \\ \delta\mathcal{D}(\hat{\rho}_S; \tilde{\gamma}) &= \sum_{j,\mu} \tilde{\gamma}_{j\mu} \left(\hat{L}_{j\mu} \hat{\rho}_S \hat{L}_{j\mu}^\dagger - \frac{1}{2} \{ \hat{L}_{j\mu}^\dagger \hat{L}_{j\mu}, \hat{\rho}_S \} \right), \end{aligned} \quad (46)$$

where index μ runs over possible decoherence processes, $\tilde{\gamma}_{j\mu}$ are their rates, and $\hat{L}_{j\mu}$ are the corresponding jump operators.

In the context of Floquet evolution, we will adopt the following simplified model: we assume that decoherence can be described by a quantum channel \mathcal{D} acting on the system after one period of Floquet evolution. The quantum channel will be constructed by considering only the dissipative part $\delta\tilde{\mathcal{D}}$ of the Lindblad generator in Eq. (46), acting over the Floquet cycle duration Δt . Experimentally, quantum processors operate in the regime where $\tilde{\gamma}_{j\mu}\Delta t \ll 1$; then, this dissipative channel can be written as (to leading order in $\tilde{\gamma}$ coefficients):

$$\mathcal{D}(\hat{\rho}_S) \approx \hat{\rho}_S + \delta\mathcal{D}(\hat{\rho}_S; \gamma), \quad (47)$$

where we introduced dimensionless decoherence rates:

$$\gamma_{j\mu} = \tilde{\gamma}_{j\mu}\Delta t, \quad \gamma_{j\mu} \ll 1. \quad (48)$$

While this approximate model is only expected to be quantitatively accurate in the Trotter limit $g, J \ll 1$, we expect it to correctly capture the qualitative effects of noise on cooling even away from that limit. The main motivation for introducing this simplified model is that it decouples the unitary evolution of the cooling protocol from the decoherence effects, leading to a transparent and compact form of the noisy kinetic equation.

Within this model, the evolution of the system-bath density matrix over one cooling period is given by:

$$\Phi^\gamma(\rho_S) = \text{Tr}_B \mathcal{D}\mathcal{M}_T \dots \mathcal{D}\mathcal{M}_1(\hat{\rho}_S \otimes \hat{\rho}_B^0), \quad (49)$$

where

$$\mathcal{M}_\tau(\cdot) = \hat{U}_{\theta, \tau} \hat{U}_B \hat{U}_S(\cdot) \hat{U}_S^\dagger \hat{U}_B^\dagger \hat{U}_{\theta, \tau}^\dagger.$$

We follow the same steps that led to Eq. (23) above, now keeping first-order terms in θ^2 and $\gamma_{j\mu}$. The processes from cooling and noise contribute independently, since we discard next-order terms $O(\gamma\theta^2)$. The change in the quasiparticle occupations due to noise takes the standard Lindblad form

$$\delta\hat{n}_k = T \sum_{j, \mu} \gamma_{j\mu} \left(\hat{L}_{j\mu}^\dagger \hat{n}_k \hat{L}_{j\mu} - \frac{1}{2} \{ \hat{L}_{j\mu}^\dagger \hat{L}_{j\mu}, \hat{n}_k \} \right), \quad (50)$$

and following Eqs. (16-23) we obtain the noisy rate equation, which includes cooling transitions $R_{\vec{\alpha}\vec{\beta}}$ and an additional contribution $R_{\vec{\alpha}\vec{\beta}}^\gamma$ to transition rates from the noise terms:

$$\delta n_k = \sum_{\vec{\alpha}, \vec{\beta}} \rho_{\vec{\alpha}\vec{\alpha}} (\beta_k - \alpha_k) [R_{\vec{\alpha}\vec{\beta}} + R_{\vec{\alpha}\vec{\beta}}^\gamma], \quad (51)$$

$$R_{\vec{\alpha}\vec{\beta}} = \theta^2 \sum_{j=1}^{N_A} |F_{h,T}(\Delta(\vec{\alpha}, \vec{\beta}))|^2 |\langle \vec{\beta} | \hat{\sigma}_{Q_j}^+ | \vec{\alpha} \rangle|^2, \quad (52)$$

$$R_{\vec{\alpha}\vec{\beta}}^\gamma = \sum_{j=1}^{N_S} \sum_{\mu} \gamma_{j\mu} T |\langle \vec{\beta} | \hat{L}_{j\mu} | \vec{\alpha} \rangle|^2. \quad (53)$$

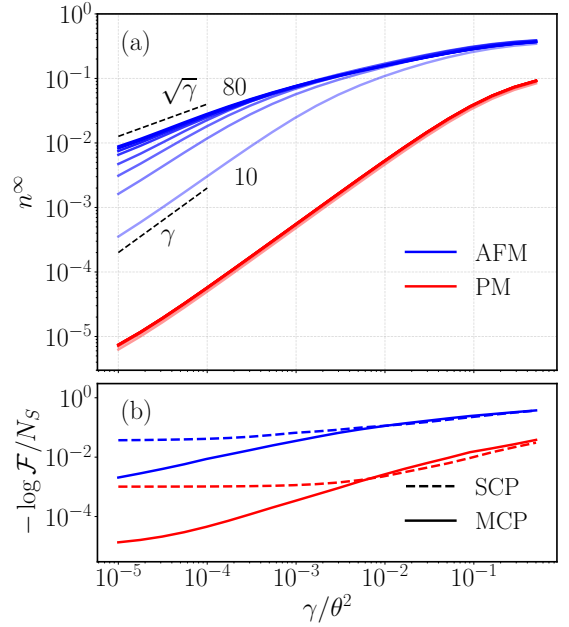


Figure 5. Performance of the cooling algorithm under decoherence. (a) Quasiparticle density in the steady state, as a function of noise ratio γ/θ^2 , in PM (red) and AFM (blue) phases, for different system sizes N_S from 10 to 80. We use MCP with fixed $T = 2\beta = 6\pi/\Delta$. At weak noise, PM quasiparticle density scales linearly with γ , while AFM displays a crossover from $n \propto \gamma$ to $n \propto \sqrt{\gamma}$ behaviour as noise strength is reduced. (b) Log-fidelity between steady state and quasiparticle vacuum, for MCP (solid lines) and SCP (dashed lines). We fix $T = 2\beta$ and optimize over parameter β for each protocol.

Note that the noise is essentially ‘infinite temperature’ and has no term analogous to the spectral filtering function $F_{h,T}$.

B. Application: cooling the transverse-field Ising model

Next, we apply the noisy kinetic equation to cooling of a transverse-field Ising model in the presence of decay to the qubit ground state, and dephasing noise. This corresponds to $\mu = d, \phi$, with jump operators

$$\hat{L}_{jd} = \hat{\sigma}_j^+, \quad \hat{L}_{j\phi} = \hat{Z}_j. \quad (54)$$

We assume homogeneous decoherence rates for simplicity, $\gamma_{j\phi} = \gamma_\phi$, $\gamma_{jd} = \gamma_d$, and rescale the dephasing rate, $\gamma_\phi \rightarrow \gamma_\phi/2$, following standard conventions in the literature on open quantum system.

Similar to our analysis in Sec. III, we restrict to processes involving at most two quasiparticle levels. (Processes involving a higher number of quasiparticles can be systematically accounted for within our formalism.) This approximation yields the same kinetic equation derived in Sec. III, Eq. (41), but with the rates modified by noise,

$W \rightarrow \tilde{W}$, $V \rightarrow \tilde{V}$:

$$\tilde{W}_k^\mp = W_k^\mp + \sum_{j=1}^{N_S} \gamma_d T |\sigma_{j;0;k}^\pm|^2 + \frac{\gamma_\phi T}{2} |Z_{j;0;k}|^2, \quad (55)$$

$$\tilde{W}_{k,q}^\mp = W_{k,q}^\mp + \sum_{j=1}^{N_S} \gamma_d T |\sigma_{j;0;k,q}^\pm|^2 + \frac{\gamma_\phi T}{2} |Z_{j;0;k,q}|^2, \quad (56)$$

$$\tilde{V}_{k,q}^\mp = V_{k,q}^\mp + \sum_{j=1}^{N_S} \gamma_d T |\sigma_{j;q;k}^\pm|^2 + \frac{\gamma_\phi T}{2} |Z_{j;q;k}|^2. \quad (57)$$

The matrix elements satisfy the selection rules discussed in Sec. III. We now summarise the main behaviour of the noisy rate equation in the two phases, with a more detailed discussion of matrix elements for \hat{Z}_j and $\hat{\sigma}_j^\pm$ operators given in Appendix D. In the PM phase, single particle loss and gain processes occur throughout the chain (cooling and decay contributions); quasiparticle pair creation/annihilation and number-conserving scattering events occur due to dephasing. In the AFM phase, on account of the domain-wall nature of excitations, only two-particle scattering and pair creation/annihilation processes can occur in the bulk, and they are induced by cooling, decay and dephasing. Single particle transitions require an interaction with the Majorana edge mode, and are localized to the chain edge.

We have compared the predictions of the noisy kinetic equation and MPS simulations in the presence of noise, finding again a good agreement in the parameter regimes accessible to MPS (moderate value of noise strength, or moderate times at a very weak noise). We refer the reader to Appendix F for a comparison of the steady state occupations, also for different coupling strengths. The rate equation, however, allows us to study system sizes and parameter regimes far beyond the reach of matrix product state simulations [67].

In Fig. 5a, we illustrate the quasiparticle density in the steady state, obtained from the kinetic equation, as a function of the noise strength. For simplicity, we choose $\gamma_d = \gamma_\phi = \gamma$ and fix auxiliary density $N_A = N_S$. We focus on the MCP with $T = 2\beta = 6\pi/\Delta$. We observe a qualitatively different behavior in the two phases, in line with above results on noiseless cooling. In the PM phase, the steady state quasiparticle density decays as a power-law function of noise, $n_{\text{PM}}^\infty \propto \gamma^a$, $a \approx 1$, with little dependence on the system size. In the AFM phase, in contrast, the density displays a power-law scaling which depends on system size, $n_{\text{AFM}}^\infty \propto \gamma^{b(N_S)}$. For small systems and weak noise, we observe similar scaling to the PM, with $b \approx 1$; as either the system size or noise strength is increased, we find a crossover to a different power $b \approx 1/2$.

The utility of the kinetic theory is demonstrated with the following simplified versions of the kinetic equations, which capture the observed features in Fig. 5a: In the PM phase, where single-quasiparticle processes can occur throughout the system (bulk and edge), the evolution of

the occupation number $n_k(t)$ is given by

$$\frac{dn_k(t)}{dt} \approx -C_1 \theta^2 n_k + C_\gamma \gamma T, \quad (58)$$

where C_1, C_γ are constants of order one. We assumed that MCP is in the regime where heating processes due to coupling to auxiliaries are strongly suppressed, and neglected the dependence of C_1, C_γ on k . For the noise we neglect terms $O(\gamma T n)$, since we are interested in the regime of weak noise and low density. Then, the expected quasiparticle density n^∞ is given by

$$n_{\text{PM}}^\infty \approx \frac{C_\gamma \gamma T}{C_1 \theta^2}, \quad (59)$$

where we averaged over k , which gives the linear dependence on $\gamma T / \theta^2$ in Fig. 5a, for weak noise.

In the AFM phase, as discussed above, the single-quasiparticle cooling processes can only occur at the edge, and their rates are suppressed by

$$\theta^2 \Gamma_k = \theta^2 C_e |u_{1,k}|^2 \approx \theta^2 C_e \frac{k^2}{N_S} \quad (60)$$

(strictly speaking, this expression holds for small quasimomenta, $k \ll 1$, but we will see below that the steady state quasiparticle density is determined mostly by this quasimomentum range). The processes removing quasiparticle pairs can be modeled by a term $-C_2 \theta^2 n_k n$, neglecting the k, q dependence of the rates $W_{k,q}^\mp$. The dominant heating mechanism is from pair creation in the bulk, $C_\gamma \gamma T (1 - n_k)(1 - n)$. Then, we arrive at

$$\frac{dn_k(t)}{dt} \approx -\theta^2 \Gamma_k n_k - C_2 \theta^2 n_k n + C'_\gamma \gamma T (1 - n_k)(1 - n). \quad (61)$$

The steady state occupation numbers are given by

$$n_k^\infty \approx \frac{C'_\gamma \gamma T}{\theta^2 \Gamma_k + C_2 \theta^2 n_{\text{AFM}}^\infty + C'_\gamma \gamma T}, \quad (62)$$

supplemented by a self-consistency condition

$$n_{\text{AFM}}^\infty = N_S^{-1} \sum_{m=1}^{N_S} n_{k_m}^\infty, \quad (63)$$

where we again neglected terms $O(\gamma T n)$ for the regime of interest. The solution $n_{\text{AFM}}^\infty(\gamma)$ exhibits two regimes, depending on the noise strength. At stronger noise values, where $n^\infty N_S \gg 1$ (such that the total number of quasiparticles in the steady state of the system is much greater than 1), two-particle cooling processes dominate. Neglecting the sub-dominant single-particle cooling contribution Γ_k yields

$$n_{\text{AFM}}^\infty \approx \left(\frac{C'_\gamma \gamma T}{C_2 \theta^2} \right)^{1/2}. \quad (64)$$

In the opposite limit, $n^\infty N_S \ll 1$, the single-particle cooling processes determine the steady state and we can neglect the C_2 term in Eq. (62). Then,

$$n_{\text{AFM}}^\infty \approx \sum_{m=1}^{N_S} \frac{C'_\gamma \gamma T}{C_e \theta^2 m^2 N_S^{-2} + C'_\gamma \gamma T N_S} \approx C \frac{\gamma T N_S^2}{\theta^2}, \quad (65)$$

with $C = \pi^2 C'_\gamma / 6 C_e$. This expression holds in the weak-noise limit, $n^\infty N_S \sim \gamma T N_S^3 / \theta^2 \ll 1$, and we made use of the approximate quantization condition $k_m \approx \pi(1 - m)/N_S$, which holds for $k_m \ll \pi$. These approximate rate equations, Eqs. (64,65), capture the crossover behaviour displayed in Fig. 5a.

In Sec. III we argued that the fidelity of the steady state with the ground state approaches 1 as the MCP parameter $T \propto \beta$ is made large. In the presence of noise, there will be an optimal T_* and β_* that maximises the fidelity, since the noise strength also scales with T . We compare the log-fidelity per qubit for the MCP and the SCP vs. the noise ratio γ/θ^2 , in Fig. 5b. For each point, we optimize the parameter β , fixing $T = 2\beta$ for simplicity (for the SCP this simply corresponds to optimizing T). We observe that, while at moderate noise values $\gamma/\theta^2 \gtrsim 10^{-2}$, the SCP marginally outperforms MCP, for weak noise the MCP reaches lower fidelities in both phases, approaching fidelity 1 as the noiseless limit is approached. We conclude that the MCP is able to prepare target states with high fidelity even in the presence of weak noise, but noise is more destructive in systems with topological excitations such as the 1d AFM example.

V. COOLING NON-INTEGRABLE SYSTEMS

In this Section, we investigate the efficiency of the MCP for preparing ground states of non-integrable models. While these models are generally thermalizing, they typically have long-lived quasiparticles at low energy density. Therefore, the theory of dissipative cooling described in the previous sections for integrable systems, is expected to hold, once the system has been cooled to a state with sufficiently low energy density.

For a numerical test, we focus on the example of the TFIM with an additional longitudinal field,

$$\hat{U}'_S = e^{-i\hat{G}_0} e^{-i\hat{G}_1}, \quad (66)$$

$$\hat{G}_0 = \frac{\pi J}{2} \sum_{i=1}^{N_S-1} \hat{X}_i \hat{X}_{i+1}, \quad \hat{G}_1 = -\frac{\pi}{2} \sum_{i=1}^{N_S} g \hat{Z}_i + g_X \hat{X}_i.$$

We fix $J = 0.1, g = g_X = 0.15$, for which the model is in a paramagnetic phase [48]. As discussed above, since quasiparticles in the PM phase are simple magnons, we expect this to be the fastest regime to cool, and simulation accuracy is higher since the system reaches the low-density regime much faster.

Our parameter choice is in the Floquet regime, and not in the strict Trotter limit ($J, g_x, g_z \ll O(1)$).

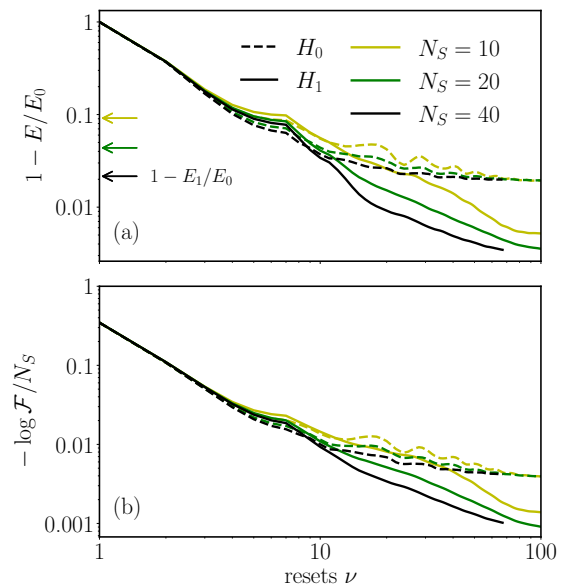


Figure 6. Cooling a non-integrable spin chain. (a) Evolution of energy, defined with respect to the ground state of approximate effective Hamiltonian H_0 (dashed lines) and H_1 (full lines), as a function of the number of resets ν , for different system sizes. Corresponding energy values for the first excited states of H_1 are indicated by arrows, showing convergence of energy to a value well below the excitation gap. (b) Log-fidelity per qubit vs. number of resets. Model parameters are $h_x = h_z = 0.15, J = 0.1$ (PM phase), reset time $T = 20 = 2\beta$. The bond dimension of simulations is $d = 300$.

Thus, to characterize the cooling efficiency, we consider effective Hamiltonians obtained in different orders of the Baker–Campbell–Hausdorff (BCH) expansion of Eq. (66), $\hat{U}'_S \approx e^{-i\hat{H}_l}$, $l = 0, 1, \dots$ (we will limit our consideration to $l = 0, 1$.) The first two orders of BCH formula give

$$\hat{H}_0 = \hat{G}_0 + \hat{G}_1, \quad \hat{H}_1 = \hat{G}_0 + \hat{G}_1 - \frac{i}{2} [\hat{G}_0, \hat{G}_1]. \quad (67)$$

The cooling efficiency can then be characterized by measuring the energy and the fidelity of the system's density matrix with respect to the ground states of the above Hamiltonians:

$$E_l = \text{tr}(\hat{H}_l \hat{\rho}), \quad \mathcal{F}_l = \langle \Omega_l | \hat{\rho} | \Omega_l \rangle, \quad (68)$$

where $l \in \{0, 1\}$ denotes the BCH expansion order, and Ω is the corresponding ground state. The system is in the prethermal regime, due to the fact that $J, g, g_X \sim O(10^{-1})$, and is expected to cool towards the ground state of an effective Hamiltonian \hat{H}_{l_*} , with an optimal truncation order $l_* \geq 1$ of the BCH series. Thus, we expect the ground state of \hat{H}_1 to provide a better approximation than that of \hat{H}_0 .

For the cooling protocol we focus on the MCP with finite density $N_A = N_S$. In contrast to the previous sections, where our aim was to develop a theory of cool-

ing, here we generalise the protocol to cool more rapidly by using a large initial value of θ , later approaching the weak coupling limit $\theta \ll 1$ where the previous analysis is expected to hold. To this end, we initialize the coupling at $\theta(0) \approx 0.4$ and progressively reduce to a final value $\theta_\infty \approx 0.083$. The value of the coupling is reduced as $\theta(t+1) = 0.8\theta(t)$ whenever the energy of the system is reduced slower than a chosen rate, $0 < E_1(t) - E_1(t-1) < 0.01$. We found this choice to be efficient for the finite time simulations. Note that the function f_τ is still modulated within a cycle, see Eq. (29). We choose a reset time $T = 20 = 2\beta$, for which $\Delta\beta \approx 2.6$, where Δ is the (many-body) energy gap of \hat{H}_1 .

The tensor-network simulations are performed similarly to the integrable case, see Appendix E for details. The ground and first excited eigenstates of \hat{H}_0 , \hat{H}_1 , and their corresponding energies, used in (68), are evaluated with a standard DMRG algorithm; the eigenstates are truncated to a bond dimension $d_0 \approx \sqrt{d}$, where d is the maximal bond dimension of the MPS performing the cooling protocol.

In Fig. 6a, we show how the energies defined with respect to \hat{H}_0 and \hat{H}_1 evolve over the course of the cooling protocol, for three different system sizes $N_S = 10, 20, 40$. We observe that the system energy decays quickly toward the ground state energy of \hat{H}_1 . (Note that due to the sweeping of θ the decay rate varies in time, as opposed to the clean exponential decay in the integrable case.) The expectation value of the zero-order Hamiltonian \hat{H}_0 saturates at a higher value than that of \hat{H}_1 , indicating that the steady-state is well-approximated by the ground state of \hat{H}_1 , as expected. Cooling efficiency appears to slightly increase with larger system sizes at later times, but larger system studies are required to provide a conclusive answer. In Fig. 6b, we observe similar behaviour in the decay of the log-fidelity per qubit, further corroborating the ability of MCP to cool the system to the ground state of an effective prethermal Hamiltonian.

These results show that the MCP remains an effective tool for cooling non-integrable systems, which exhibit long-lived quasiparticles at a sufficiently low energy density. We expect that the performance of cooling protocols can be further improved, e.g. by adapting methods employed in variational quantum algorithms [68].

VI. DISCUSSION AND OUTLOOK

In summary, in this work we investigated cooling protocols for preparing ground states of many-body systems on quantum processors. Our approach is reminiscent of cooling strategies in systems of ultracold atoms, including sympathetic cooling [69], but our protocol primarily aims to remove quasiparticles – emergent excitations above a many-body ground state. We developed a phenomenological kinetic theory framework, which accounts for competing cooling and heating processes induced by auxiliaries and by noise, and compared the efficiency of

different cooling protocols.

Our results are directly applicable to studying correlated states with current digital quantum processors, as well as in analog processors with the fast reset capability: indeed, SCP was recently implemented on the Google Quantum Processor [38]. While reaching the ground state in that experiment was challenging due to the level of noise $\gamma \approx 0.01$, our work shows that, with e.g. $\theta = 0.1$, noise values of $\gamma \approx 10^{-3}$ will be sufficient for preparing steady states with quasiparticle density below $n \approx 10^{-2}$ in the paramagnetic phase (see Fig. 5b). In systems of $N_S = 100$ qubits, this translates to approximately one quasiparticle in the sample. Cooling the antiferromagnetic phase is more challenging; nevertheless, noise level $\gamma \approx 10^{-6}$ allows to reach comparable densities. We expect that such low-energy states can be further efficiently purified to extract properties of the ground state and low-energy dynamics [38].

The quasiparticle cooling algorithm is a promising alternative to existing state-preparation methods, including variational unitary circuits [19–21], thanks to a degree of robustness with respect to noise it offers, as well as its generality. First, dissipation removes excitations created by noise, and the steady state is independent of the initial state and the history of errors. Second, our study of non-integrable TFIM suggests that the cooling approach may be suitable for preparing a broad class of correlated states in non-integrable systems. We note that the cooling algorithm requires the ability to engineer a local coupling operator which has a non-zero overlap with quasiparticle operators. Developing strategies to identify efficient auxiliary-system coupling for models of quantum magnetism, in particular in 2d, is an important direction for future research.

Despite the generality of this approach, we expect certain states will yet prove hard to prepare. One reason is that preparing ground states with high fidelity in general would allow one to solve QMA-complete problems [70], which would contradict a widely believed conjecture that QMA-complete problems cannot be solved efficiently on quantum computers. Still, we do not expect the extreme hard cases to arise in the absence of spin-glass order. In this context, it is therefore important to understand which phases of matter can be prepared by the quasiparticle cooling and other dissipative algorithms.

As pointed out in Ref. [43], and further highlighted by our analysis, systems with topological, non-local quasiparticles are more challenging to cool. On the fundamental level, this stems from lower bounds [71, 72] on the preparation times of topologically ordered states (e.g., toric code). Exploring strategies of optimal cooling of such systems, for example by creating quasiparticle traps or making use of dynamical gauge fields [73], is a promising direction of future research. Furthermore, it would be interesting to apply our analysis to quantum-critical points with gapless quasiparticles, and to study the possibility of cooling strongly interacting systems without long-lived quasiparticles. Generally, we may expect [74]

that algorithms similar to ours will be able to efficiently prepare low-energy states of *thermalizing systems* (which rules out examples such as spin glasses, where cooling procedure will drive the system to one of the many metastable minima).

Our work suggests several other avenues for future research. First, we note that our protocol may be modified to prepare approximate finite-temperature Gibbs states [27, 34, 74, 75], by appropriately choosing the filter function and the operator entering coupling to auxiliary, such that the corresponding rates in Eqs. (42-44) approximately satisfy the detailed balance condition. In fact, this is achieved by our MCP, Eq. (29), see Appendix B, giving a corresponding effective temperature $T_{\text{eff}} = 1/2\beta$. Weak noise processes in quantum processors generally violate detailed balance, and will make the steady state slightly non-thermal. In contrast, intrinsic thermalization mechanisms in interacting systems are expected to favor the thermal state. This competition, and the resulting steady state may be studied using digital [38] and analog quantum processors.

Finally, our protocol can be modified to engineer non-equilibrium quasiparticle distribution in the steady state.

Appendix A: Details of modulated coupling pulse

In this Appendix, we provide additional details regarding the modulated coupling protocol (MCP) defined in Eq. (29). As explained in Section II, this pulse is advantageous in that the corresponding filter function, $F_{h,T}(\epsilon)$, approximates a broadened step function, with broadening controlled by the parameter β . This can be seen as follows: Recalling the definition of the filter function (Eq. 24), we have for the MCP

$$F_{h,T}(\epsilon) = \frac{\pi}{A\beta} \sum_{\tau=1}^T \frac{\sin[\pi(\tau - \tau_0)/2]}{\sinh[\pi(\tau - \tau_0)/\beta]} e^{i\tau(\epsilon - \pi h)}. \quad (\text{A1})$$

For the MCP we choose the auxiliary field $h = 1/2$. We consider the limits $T, \beta \rightarrow \infty$, with the ratio $\alpha = \beta/T \ll 1$ held constant. Then, the summation (A1) can be replaced with the integral

$$\frac{\pi}{A} \int_{-1/2\alpha}^{1/2\alpha} dz \frac{e^{i\epsilon\beta z} - e^{i(\epsilon - \pi)\beta z}}{2 \sinh(\pi z)}, \quad (\text{A2})$$

up to an unimportant phase factor. For $\alpha \ll 1$ the integral limits can be extended to infinity and (A2) evaluated via residues, giving ($\epsilon > 0$)

$$F_{h,T}(\epsilon) = \pi \left[\frac{\tanh(\epsilon\beta/2) - \tanh((\epsilon - \pi)\beta/2)}{\tanh(\pi\beta/4)} \right]. \quad (\text{A3})$$

Here we used the normalization condition $\sum_{\tau=1}^T f_{\tau} = 1$. The expression for $\epsilon < 0$ follows from the residue formula $F(\epsilon) + F(-\epsilon) = 2\pi$.

The properties of the steady state, and evolution towards it can give useful insights into interactions between quasiparticles, their dynamics, and lifetimes – properties that play a central role in our understanding of correlated materials. We note that the accuracy of the kinetic theory we used to model the cooling protocol suggests that the dominant thermalization mechanisms are well approximated by few-particle processes. Applications of suitably modified protocols in quantum simulator experiments would unlock new avenues to study underlying dynamics and thermalization mechanisms.

ACKNOWLEDGMENTS

We thank Zala Lenarčič, Iris Ulčakar and Guifre Vidal for insightful discussions, and Rolando Somma and Guifre Vidal for useful comments on the manuscript. This work was partially supported by the European Research Council via the grant agreements TANQ 864597 (A.M., D.A.).

The ratio

$$\left| \frac{F_{h,T}(+\epsilon)}{F_{h,T}(-\epsilon)} \right| = \left| \frac{\tanh(\epsilon\beta/2) - \tanh((\epsilon - \pi)\beta/2)}{\tanh(\epsilon\beta/2) - \tanh((\epsilon + \pi)\beta/2)} \right| \quad (\text{A4})$$

$$\approx e^{\epsilon\beta},$$

gives the detailed balance condition when $\pi\beta \gg \max(1, \epsilon\beta)$. This condition ensures heating transitions are exponentially less frequent than the cooling transitions of the same energy.

In Fig. 7 we compare $|F_{h,T}(\epsilon)|$ obtained from the integral approximation, (A3), and the exact sum (A1). We take $\beta = 10$ and show the summation result for $T = 2\beta$. Even for this relatively small value of T/β (or, equivalently, relatively large $\alpha = 0.5$), Eq. (A3) clearly captures the main behaviour of the filter function. The main discrepancy is due to small oscillations (‘ringing’) on top of the integral result. These finite-time artifacts can be viewed as errors arising from the truncation of the Fourier series limits in Eq. (A1) at finite T . For large T/β , this ringing error is bounded approximately as

$$|F_{h,T}(\epsilon) - F_{h,\infty}(\epsilon)| \lesssim \frac{\exp(-\pi T/\beta)}{A}. \quad (\text{A5})$$

In realistic systems the errors due to noise will typically be much larger than the above truncation errors, and we can obtain efficient cooling with values of T, β , considered in the main text.

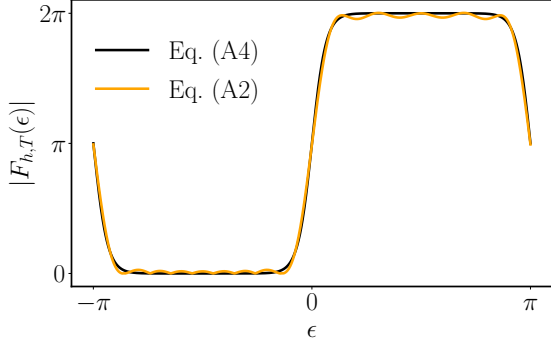


Figure 7. Comparison of integral approximation for $F_{h,T}(\epsilon)$ (Eq. A3, black) and exact summation (Eq. A1, orange), for parameters $\beta = 10$, $T = 2\beta$.

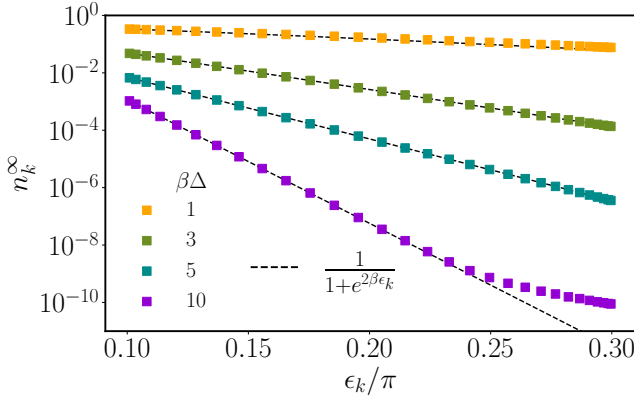


Figure 8. Steady state quasiparticle populations for cooling with thermal MCP, for effective temperature $T_{\text{eff}} = 1/2\beta$. Results shown are for PM phase with one auxiliary per site, with system size $N_S = 30$ and reset time $T = 5\beta$. The dashed black lines are the expected thermal (Fermi) distributions.

Appendix B: Detailed balance and thermal state preparation with MCP

Above, we focused on preparation of ground states, which corresponds to the limit $\beta\Delta \rightarrow \infty$, where Δ is the quasiparticle gap. However, our MCP protocol also provides a way to prepare *thermal states* (finite temperature Gibbs states) of the same effective Hamiltonian, a subject which has been the focus of several recent studies [27, 34, 74, 76]. The thermal Gibbs state at an effective temperature T_{eff} is defined by

$$\frac{\rho_{\vec{\alpha}\vec{\alpha}}}{\rho_{\vec{\beta}\vec{\beta}}} = \exp\left(-\frac{\varepsilon(\vec{\alpha}) - \varepsilon(\vec{\beta})}{T_{\text{eff}}}\right), \quad (\text{B1})$$

where $\rho_{\vec{\alpha}\vec{\alpha}}$ are the many-body populations in Eq. (19), ε is the total quasienergy of the many-body eigenstate.

This can be achieved by cooling the system using the MCP with the parameter $\beta = 1/2T_{\text{eff}}$, and the additional constraint that the coupling operators V_j appearing in Eq. (8) are *Hermitian*. Then, the general rate equation, Eq. (23), replacing $\hat{\sigma}_j^\pm$ with the Hermitian operators V_j ,

can be written as

$$\delta n_k = \frac{1}{2} \sum_{\vec{\alpha}\vec{\beta}} (\beta_k - \alpha_k) w_{\vec{\alpha}\vec{\beta}} \left(\rho_{\vec{\alpha}\vec{\alpha}} - \rho_{\vec{\beta}\vec{\beta}} \frac{w_{\vec{\beta},\vec{\alpha}}}{w_{\vec{\alpha}\vec{\beta}}} \right) \quad (\text{B2})$$

where

$$w_{\vec{\alpha}\vec{\beta}} = |F_{h,T}(\Delta(\vec{\alpha}, \vec{\beta}))|^2 |\langle \vec{\beta} | V_j | \vec{\alpha} \rangle|^2, \quad (\text{B3})$$

and $\Delta(\vec{\alpha}, \vec{\beta}) = \varepsilon(\vec{\alpha}) - \varepsilon(\vec{\beta})$ are the Bohr frequencies. If the *detailed balance* condition holds, that is, when the terms inside the bracket above vanish identically,

$$\frac{\rho_{\vec{\alpha}\vec{\alpha}}}{\rho_{\vec{\beta}\vec{\beta}}} = \frac{|F_{h,T}(\Delta(\vec{\beta}, \vec{\alpha}))|^2 |\langle \vec{\alpha} | V_j | \vec{\beta} \rangle|^2}{|F_{h,T}(\Delta(\vec{\alpha}, \vec{\beta}))|^2 |\langle \vec{\beta} | V_j | \vec{\alpha} \rangle|^2}, \quad (\text{B4})$$

then this provides a solution to the steady state $\delta n_k = 0$. With the Hermitian constraint and choice $\beta = 1/2T_{\text{eff}}$, using the asymptotic form of the filter function Eq. (A4) gives the required Gibbs state, Eq. (B1).

As a demonstration, we calculate the steady state quasiparticle populations from the rate equation in the PM phase of the Floquet TFIM, with one auxiliary per site and keeping single-particle processes as in Section III. We choose hermitian operators $V_j = \hat{Z}_j$. The results are shown in Fig. 8, for several values of the inverse temperature β . We take system size $N_S = 30$ and $T = 5\beta$ to reduce ringing artifacts. The results are compared to the expected Fermi distributions which hold for fermionic quasiparticles when Eq. (B1) is satisfied; the agreement is generally excellent, suggesting that thermal Gibbs states can be efficiently prepared by the quasiparticle cooling algorithm (where, as in the ground state case, errors due to noise etc. will result in slightly non-equilibrium steady state populations).

Appendix C: Quasiparticles in the TFIM

The Floquet TFIM with open boundary conditions, considered as our cooling example throughout the main text, is defined by the Floquet unitary

$$\hat{U}_S = \exp\left(-\frac{i\pi J}{2} \sum_{i=1}^{N_S-1} \hat{X}_i \hat{X}_{i+1}\right) \exp\left(\frac{i\pi g}{2} \sum_{i=1}^{N_S} \hat{Z}_i\right). \quad (\text{C1})$$

This model can be mapped onto a quadratic fermionic chain by the Jordan-Wigner mapping, Eq. (32). For this purpose it is convenient to introduce a basis of Hermitian Majorana fermion operators, defined as

$$\hat{a}_{2i-1} = \hat{c}_i + \hat{c}_i^\dagger, \quad \hat{a}_{2i} = i(\hat{c}_i^\dagger - \hat{c}_i). \quad (\text{C2})$$

Then the unitary \hat{U}_S acts on Majorana operators as a linear transformation:

$$\hat{U}_S^\dagger \hat{a}_i \hat{U}_S = \sum_{j=1}^{2N_S} (K_S)_{ij} \hat{a}_j. \quad (\text{C3})$$

From Eq. (C1) we find the K_S matrix given by

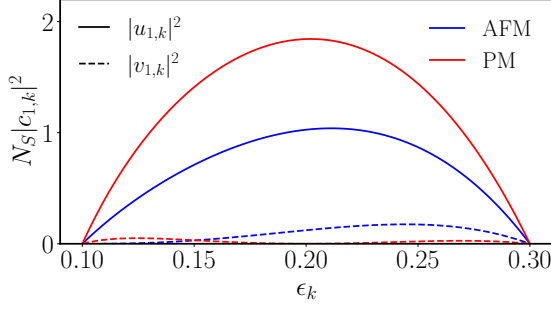


Figure 9. Profile of edge Bogoliubov coefficients $|u_{1k}|^2$, (solid) $|v_{1k}|^2$ (dashed), plotted vs quasienergy ϵ_k . We plot the coefficients rescaled by chain length N_S : squared coefficients are $O(1/N_S)$ in middle of quasiparticle band, but vanish as $O(1/N_S^3)$ at band edges.

$$K_S = \begin{pmatrix} 1 & 0 & 0 & \dots & 0 \\ 0 & \cos \pi J & -\sin \pi J & \dots & 0 \\ 0 & \sin \pi J & \cos \pi J & \dots & 0 \\ \vdots & \vdots & \vdots & \ddots & \vdots \\ 0 & 0 & 0 & 0 & 1 \end{pmatrix} \begin{pmatrix} \cos \pi g & \sin \pi g & 0 & 0 & \dots \\ -\sin \pi g & \cos \pi g & 0 & 0 & \dots \\ 0 & 0 & \cos \pi g & \sin \pi g & \dots \\ 0 & 0 & -\sin \pi g & \cos \pi g & \dots \\ \vdots & \vdots & \vdots & \vdots & \ddots \end{pmatrix}. \quad (\text{C4})$$

The eigenmodes of \hat{U}_S are Dirac fermions satisfying

$$\hat{U}_S^\dagger \hat{\eta}_k \hat{U}_S = e^{-i\epsilon_k} \hat{\eta}_k, \quad (\text{C5})$$

where k is a quantum number labeling the eigenmodes (the quasimomentum). Defining the eigenvectors of K_S (for $\epsilon_k \geq 0$) according to

$$K_S \psi_k = e^{-i\epsilon_k} \psi_k, \quad (\text{C6})$$

we have the expansion

$$\hat{\eta}_k = \frac{1}{\sqrt{2}} \sum_{j=1}^{N_S} \psi_{k,2j-1}^* \hat{a}_{2j-1} + \psi_{k,2j}^* \hat{a}_{2j}. \quad (\text{C7})$$

Due to particle-hole symmetry, the eigenvectors of K_S with negative quasienergy are related to those of positive quasienergy by the conjugation $\varphi_k = \psi_k^*$, $K_S \varphi_k = e^{i\epsilon_k} \varphi_k$. The eigenvectors ψ_k and quasienergies ϵ_k can be found by exact diagonalisation of the K_S matrix; in Appendix A of Ref. [38], an analytical derivation was also given. Note that the boundary condition defines the quantization condition for the N_S quasimomenta k_m , in terms of which the quasienergies are given by the exact formula

$$\cos \epsilon_k = \cos(\pi J) \cos(\pi g) - \sin(\pi J) \sin(\pi g) \cos k. \quad (\text{C8})$$

Along with the definition of the Bogoliubov coefficients,

$$\hat{c}_j = \sum_k u_{jk} \hat{\eta}_k + v_{jk} \hat{\eta}_k^\dagger, \quad (\text{C9})$$

this gives the relations

$$u_{jk} = \frac{\psi_{k,2j-1} + i\psi_{k,2j}}{\sqrt{2}}, \quad (\text{C10})$$

$$v_{jk} = \frac{\psi_{k,2j-1}^* + i\psi_{k,2j}^*}{\sqrt{2}}, \quad (\text{C11})$$

specifying the standing-wave form of the eigenmodes.

Since the Bogoliubov coefficients at the boundary play a particularly important role in the cooling rates entering the kinetic equation for edge cooling, we plot the values of $|u_{1k}|^2$, $|v_{1k}|^2$ in Fig. 9, vs. the quasienergy ϵ_k . We observe that quasiparticle in the middle of the band typically have boundary overlap $|u_{1k}|^2 = O(N_S^{-1})$, while the overlap vanishes for quasiparticles with quasienergy near the two band edges. The overlap for these quasiparticles is expected to go as $O(N_S^{-3})$ [59].

Appendix D: Matrix elements for bulk cooling

In Sections III, IV, we considered cooling in the example of the transverse-field Ising model, with two types of matrix elements appearing in the derivation of the rate equations: the \hat{Z}_j matrix elements, which we denote as

$$Z_{j;\vec{\alpha};\vec{\beta}} = \langle \vec{\alpha} | \hat{Z}_j | \vec{\beta} \rangle, \quad (\text{D1})$$

and the $\hat{\sigma}_j^\pm$ matrix elements,

$$\sigma_{j;\vec{\alpha};\vec{\beta}}^\pm = \langle \vec{\alpha} | \hat{\sigma}_j^\pm | \vec{\beta} \rangle. \quad (\text{D2})$$

Here $|\vec{\alpha}\rangle$ are the many-body eigenstates of the TFIM, which are completely defined by their quasiparticle occupation numbers.

Although TFIM defines an integrable model, calculation of spin matrix elements can be challenging [77], due to the fact that the Jordan-Wigner transformation

between spin and fermion operators is non-local. We will see that this is the case for the $\hat{\sigma}_j^\pm$ matrix elements below.

First, we focus on the simpler case of \hat{Z}_j :

1. $Z_{j;\vec{\alpha};\vec{\beta}}$ matrix elements

In the fermion basis \hat{Z} is a quadratic operator, so only matrix elements between eigenstates differing in the occupation of at most two quasiparticle modes survive:

$$\begin{aligned} Z_{j;\vec{\alpha};\vec{\beta}} &= \langle \vec{\alpha} | (1 - 2\hat{c}_j^\dagger \hat{c}_j) | \vec{\beta} \rangle \\ &= \delta_{\vec{\alpha}\vec{\beta}} - 2 \sum_{kq} \left(u_{jk}^* u_{jq} [\hat{\eta}_k^\dagger \hat{\eta}_q]_{\vec{\alpha}\vec{\beta}} + u_{jk}^* v_{jq} [\hat{\eta}_k^\dagger \hat{\eta}_q^\dagger]_{\vec{\alpha}\vec{\beta}} + v_{jk}^* u_{jq} [\hat{\eta}_k \hat{\eta}_q]_{\vec{\alpha}\vec{\beta}} + v_{jk}^* v_{jq} [\hat{\eta}_k \hat{\eta}_q^\dagger]_{\vec{\alpha}\vec{\beta}} \right) \end{aligned} \quad (\text{D3})$$

where e.g. $[\hat{\eta}_k^\dagger \hat{\eta}_q]_{\vec{\alpha}\vec{\beta}} \equiv \langle \vec{\alpha} | \hat{\eta}_k^\dagger \hat{\eta}_q | \vec{\beta} \rangle = 0, 1$ is only non-zero if $\vec{\alpha}$ and $\vec{\beta}$ differ only by the occupations of the k and q quasiparticle levels (including the case $k = q$). Since the Bogoliubov coefficients u_{jk}, v_{jk} can be obtained by diagonalisation of the single-particle Hamiltonian, the matrix elements are easily obtained.

In deriving the rate equation, we focused on the case of transitions to and from the ground state, and scattering between single quasiparticle levels. Thus we have

$$|Z_{j;0;k,q}|^2 = |\langle \Omega | \hat{Z}_j | k, q \rangle|^2 = 4|v_{jk}^* u_{jq}|^2 \quad (\text{D4})$$

as the probability for two quasiparticles with quasimomenta k, q , to annihilate, and

$$|Z_{j;k;q}|^2 = |\langle k | \hat{Z}_j | q \rangle|^2 = 4|u_{jk}^* u_{jq}|^2 \quad (\text{D5})$$

as the scattering probability $q \rightarrow k$. Since \hat{Z} is hermitian, the pair-creation probability is equal to the pair-annihilation, i.e. $|Z_{j;0;k,q}|^2 = |Z_{j;k,q;0}|^2$. Note that, in the AFM phase there is also an amplitude for single-quasiparticle processes, due to the selection rules discussed in the main text i.e. one of k, q can be taken as the Majorana zero mode.

2. $\sigma_{j;\alpha;\beta}^\pm$ matrix elements

We now turn to quasiparticle processes mediated by the $\hat{\sigma}_j^\pm$ matrix elements. We focus on $\hat{\sigma}_j^-$ for illustration. In the fermion basis, $\hat{\sigma}_j^-$ comes attached with the Jordan-Wigner string operator,

$$\sigma_{j;\vec{\alpha};\vec{\beta}}^- = \langle \vec{\alpha} | \left(\prod_{i=1}^{j-1} e^{i\pi \hat{c}_i^\dagger \hat{c}_i} \right) \hat{c}_j^\dagger | \vec{\beta} \rangle. \quad (\text{D6})$$

Due to this non-locality in the fermionic eigenbasis, multi-particle processes are allowed with $\hat{\sigma}_j^-$ changing

the occupation numbers of up to $2j - 1$ quasiparticle levels. Amazingly, the exact finite-volume matrix elements have been worked out for the case of the \hat{X}_j operators in the TFIM with periodic boundary conditions [77]. Here, we focus on single- and two-particle transitions near the ground state, which capture the dominant cooling processes at late times, as described in the main text. Our theory can be straightforwardly generalised to include higher-order processes.

Focusing on few-particle processes allows us to use Wick's theorem to evaluate the necessary matrix elements for systems up to several hundred sites: For free (more generally, Gaussian) theories, Wick's theorem states that

$$\begin{aligned} \langle \hat{a}_{i_1} \hat{a}_{i_2} \dots \hat{a}_{i_{2N}} \rangle_\Omega &= \sum_P \zeta_P \prod_{k=1}^N \langle \hat{a}_{P(i_{2k-1})} \hat{a}_{P(i_{2k})} \rangle \quad (\text{D7}) \\ &= \text{Pf} \begin{pmatrix} 0 & \langle \hat{a}_{i_1} \hat{a}_{i_2} \rangle & & & \\ & 0 & \langle \hat{a}_{i_1} \hat{a}_{i_3} \rangle & \dots & \langle \hat{a}_{i_1} \hat{a}_{i_{2N}} \rangle \\ & & \langle \hat{a}_{i_2} \hat{a}_{i_3} \rangle & \dots & \langle \hat{a}_{i_2} \hat{a}_{i_{2N}} \rangle \\ & & & 0 & \dots & \langle \hat{a}_{i_3} \hat{a}_{i_{2N}} \rangle \\ & & & & \ddots & \vdots \\ & & & & & 0 \end{pmatrix}. \quad (\text{D8}) \end{aligned}$$

The sum runs over all possible permutations of the Majorana indices, and $\zeta_P = \pm 1$ is the sign of the permutation, carrying the fermion statistics. All expectation values are taken with respect to the ground state of the free theory, and for notational simplicity we introduced the Majorana fermion operators (Eq. (C2)). In the second line we introduced the Pfaffian representation of Wick's theorem in terms of a skew-symmetric matrix Σ . In our case, since only the modulus squared of the correlation functions enters the rate equation, we may use

$$|\langle a_{i_1} a_{i_2} \dots a_{i_{2N}} \rangle_\Omega|^2 = |\text{Pf}(\Sigma)|^2 = |\det(\Sigma)|. \quad (\text{D9})$$

which can be computed in time $O(N^3)$. For further reference, see e.g. [61, 78].

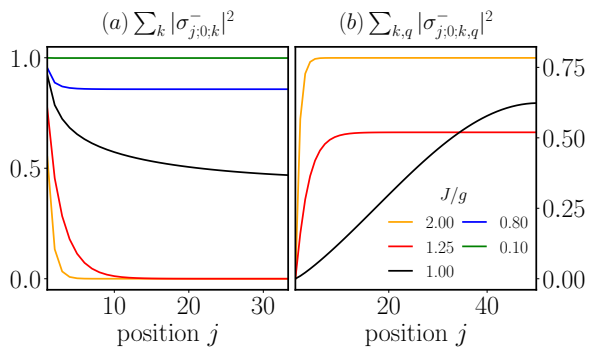


Figure 10. (a) Single-quasiparticle matrix elements $|\sigma_{j0k}^-|^2$ summed over quasimomenta k and plotted against operator position j , for different values of J/g . (b) Two-particle matrix elements $|\sigma_{j0(k,q)}^-|^2$ summed over k, q , and plotted against operator position j . Note that the two-particle matrix element is non-zero only in the AFM phase.

Single quasiparticle processes: We first consider single-quasiparticle transitions above the ground state,

$$\sigma_{j;0;k}^- = \langle \Omega | \hat{\sigma}_j^- | k \rangle \quad (\text{D10})$$

being the amplitude to directly excite a quasiparticle of quasimomentum k . We rewrite the single-particle element in fermion basis

$$|\sigma_{j;0;k}^-|^2 = \left| \langle \prod_{i=1}^{j-1} \hat{a}_{2i-1} \hat{a}_{2i} \hat{c}_j^\dagger \hat{\eta}_k^\dagger \rangle_{\Omega} \right|^2. \quad (\text{D11})$$

The corresponding Wick's matrix Σ had dimension $2j \times 2j$. In Fig. 10a we show how the single-particle matrix elements in Eq. D11 (summed over k), depend on the TFIM phase parameter J/g and on the position of the operator j . The system size is $N_S = 100$. The matrix elements display a clear change in behaviour between the two phases: in the PM phase, single-particle transitions occur almost uniformly throughout the system bulk; in the AFM phase, transitions are localized within a few correlation lengths of the edge, with a correlation length $\xi_J \propto J/g$. This is as expected, based on the physical picture of domain-wall-like quasiparticles in the AFM (removing a single domain wall requires flipping a macroscopic number of spins).

Two-quasiparticle processes: Based on the physical picture, we expect that in the AFM phase, a pair of domain walls may collide in the bulk and annihilate, as this requires only local reconfigurations of spins. However, there is a subtlety, from the fact that $\hat{\sigma}_j^-$ has non-zero matrix elements only between eigenstates of different fermion parity. This rules out two-particle transitions in the PM phase, but as discussed in the main text, the issue is sidestepped in the AFM by interacting with the Majorana zero mode, whose action maps between the two

nearly-degenerate ground states. We therefore write

$$|\sigma_{j;0;k,q}^-|^2 = \left| \langle \Omega_+ | \prod_{i=1}^{j-1} \hat{a}_{2i-1} \hat{a}_{2i} \hat{c}_j^\dagger \hat{\eta}_k^\dagger \hat{\eta}_q^\dagger | \Omega_- \rangle \right|^2, \quad (\text{D12})$$

with $|\Omega_- \rangle = \hat{\eta}_0^\dagger |\Omega_- \rangle$, and $\hat{\eta}_0^\dagger$ the Majorana mode. These matrix elements may be evaluated with Wick's theorem on the $(2j+2) \times (2j+2)$ dimensional Σ -matrix. In Fig. 10b, we show how the summed matrix elements $\sum_{k,q} |\sigma_{j;0;k,q}^-|^2$ depend on the position j , for different values of J/g in the AFM phase. The pair matrix element is almost homogeneous in the bulk, vanishing in the edge region.

For completeness we also give the two-particle scattering elements, which are again non-zero only for the AFM phase:

$$|\sigma_{j;k;q}^-|^2 = \left| \langle \Omega_+ | \hat{\eta}_k \prod_{i=1}^{j-1} \hat{a}_{2i-1} \hat{a}_{2i} \hat{c}_j^\dagger \hat{\eta}_q^\dagger | \Omega_- \rangle \right|^2. \quad (\text{D13})$$

The scattering does not directly lead to cooling/heating of the system (the total number of quasiparticles is conserved by the scattering processes), however it can lead to a redistribution of quasiparticle density, which itself affects the cooling rate.

Appendix E: Details of numerical simulations

1. Free fermion simulations

For the edge cooling protocol analysed in Section III for the TFIM, the non-unitary dynamics described by Eq. (1) defines a Gaussian channel — a channel mapping Gaussian states to Gaussian states. A Gaussian state obeys Wick's theorem (see Eq. D8), meaning that the expectation values of all observables can be factorised purely in terms of 2-point fermionic correlation functions. Under the action of the cooling channel, Eq. (1), the matrix of 2-point functions can be efficiently updated, as we show below, and hence we have access to the arbitrary correlators of the time-dependent many-body state.

We introduce the antisymmetrised covariance matrix of Majorana correlators as

$$\Gamma_{ij} = \frac{i}{4} \langle [\hat{a}_i, \hat{a}_j] \rangle = \begin{cases} i \langle \hat{a}_i \hat{a}_j \rangle / 2, & i \neq j \\ 0, & i = j \end{cases}, \quad (\text{E1})$$

where the Majorana fermions were defined in Eq. (C2). The matrix includes both system and bath degrees of freedom, and has dimension $(2N_S + 2) \times (2N_S + 2)$ (we limit our discussion to the case of a single edge auxiliary for simplicity). We block the covariance matrix according to

$$\Gamma = \begin{pmatrix} \Gamma_{BB} & \Gamma_{SB} \\ \Gamma_{BS} & \Gamma_{SS} \end{pmatrix}. \quad (\text{E2})$$

where Γ_{SS} is the $2N_S \times 2N_S$ matrix containing system-system correlations, etc. For the initial condition, representing the system in the maximally mixed state and the auxiliary in the reset state, Eq. (6), we have

$$\Gamma_{SS} = 0 \quad (\text{E3})$$

$$\Gamma_{BB} = \frac{1}{2} \begin{pmatrix} 0 & -1 \\ 1 & 0 \end{pmatrix}, \quad \Gamma_{SB} = \Gamma_{BS} = 0. \quad (\text{E4})$$

Due to the integrability of the TFIM, unitary evolution of the Majoranas in the Heisenberg picture acts as a linear map:

$$(\hat{U}_S^\dagger \hat{U}_B^\dagger \hat{U}_\theta^\dagger) \hat{a}_i (\hat{U}_\theta \hat{U}_B \hat{U}_S) = \sum_j (K_\theta K_B K_S)_{ij} \hat{a}_j, \quad (\text{E5})$$

where K_S is defined in (C4), and $K_B = \exp(\pi h_B)$, $K_\theta = \exp(\pi h_\theta)$, with

$$h_B = \begin{pmatrix} 0 & h & 0 & \dots \\ -h & 0 & 0 & \dots \\ 0 & 0 & 0 & \dots \\ \vdots & \vdots & \vdots & \ddots \end{pmatrix}, \quad h_\theta = \begin{pmatrix} 0 & 0 & 0 & \theta & \dots \\ 0 & 0 & -\theta & 0 & \dots \\ 0 & \theta & 0 & 0 & \dots \\ -\theta & 0 & 0 & 0 & \dots \\ \vdots & \vdots & \vdots & \vdots & \ddots \end{pmatrix}, \quad (\text{E6})$$

all other elements being zero. Then, defining $\hat{U} = \hat{U}_\theta \hat{U}_B \hat{U}_S$ and $K = K_\theta K_B K_S$, the covariance matrix evolves under the unitary part of the cooling channel as,

$$\langle \hat{U}^\dagger \hat{\Gamma}_{ij} \hat{U} \rangle = K_{il} K_{jm} \langle [\hat{a}_l, \hat{a}_m] \rangle = (K \Gamma K^T)_{ij}. \quad (\text{E7})$$

The reset of the auxiliaries can be done by reinstating condition (E4). If we denote the corresponding map by \mathcal{R} , then the cooling channel (1) acts on the covariance matrix according to (in a slight abuse of notation):

$$[\Phi(\Gamma)]_{ij} = [\mathcal{R}(K \Gamma K^T)]_{ij}. \quad (\text{E8})$$

Thus the matrix Γ can be efficiently updated to obtain the dynamics, or (by vectorising the matrix Γ) the linear map Φ diagonalised to yield the steady state. Note that qubit dephasing can also be efficiently implemented in this scheme [79], but bulk auxiliaries or qubit decay break the necessary integrability.

2. Tensor network simulations

Here, we summarize the tensor network algorithm that was employed to simulate the dissipative dynamics in Sections III-V. We give an overview of the relevant details, assuming the reader is familiar with the basics of matrix product algorithms; introductions can be found in e.g. [80, 81].

We assume a finite density of auxiliaries, one per system site. The total density matrix of the system plus auxiliaries is ρ_{SB} . We work with the vector unfolding of

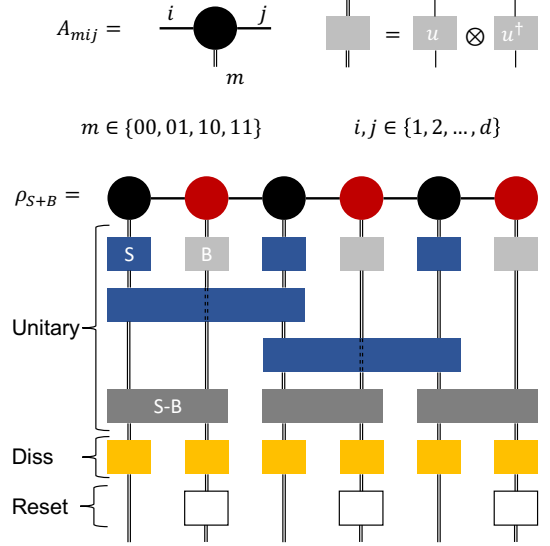


Figure 11. Tensor network implementation for one cooling cycle. System (auxiliary) qubits are denoted by black (red) tensors respectively. Different channels correspond to different blocks: bath evolution (light grey); system evolution (dark blue); system-bath coupling (dark grey); decoherence (yellow); auxiliary reset (white). The network is composed of rank-3 tensors A , has a bond dimension d and a 4-dimensional physical bond corresponding to the four (vectorised) states of the qubit's density matrix. The system is encoded in a one-dimensional geometry at the price of introducing next-nearest neighbor channels.

the density matrix product operator, which is written as a matrix product state (MPS),

$$\rho_{SB} = \sum_{\mathbf{m}, \mathbf{s}} A_{m_1, s_1}^1 A_{m_2, s_1, s_2}^2 \dots A_{m_N, s_{N-1}}^N |m_1 \dots m_N\rangle, \quad (\text{E9})$$

where A^i is a rank-3 tensor graphically defined in Fig. 11. Virtual indices $\mathbf{s} = \{s_1, \dots, s_{N-1}\}$ are traced while physical indices $\mathbf{m} = \{m_1, \dots, m_N\}$ denote the different states of the system+bath, $N = 2N_S$. The system geometry in the presence of auxiliaries is quasi-1d, see Fig. 1d, and we adopt a 1-dimensional ordering that alternates between system and auxiliary qubits i.e. $\mathcal{Q}_1 \mathcal{A}_1 \dots \mathcal{Q}_{N_S} \mathcal{A}_{N_S}$, as illustrated in Fig. 11. The dimension of the virtual indices of the MPS (bond dimension) is denoted d , and controls the amount of non-local correlations that can be represented by the state.

The time evolution is performed via the standard TEBD algorithm [64, 65], which updates the MPS in real time, followed by the reset channel acting on the bath, which can be efficiently implemented as discussed below. In Fig. 11 we illustrate the evolution for the example of the Floquet TFIM (5) with bath evolution and interaction, Eqs. (7-10). We first simultaneously perform the single-site unitary channels for the system and bath, then the two-body system gates, which correspond to next-nearest-neighbor gates, followed by

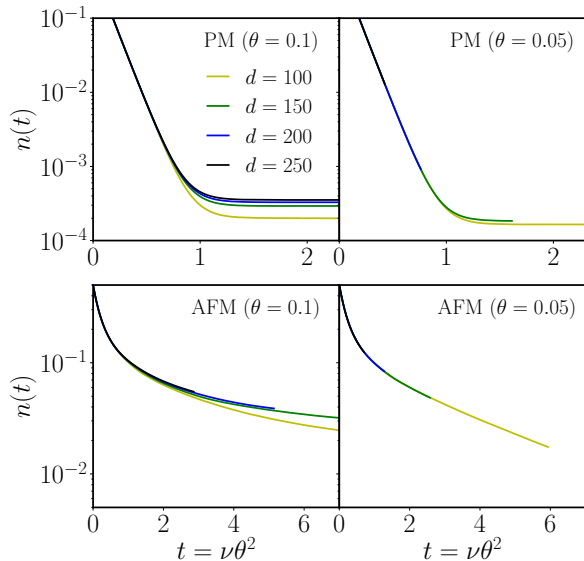


Figure 12. Convergence of ground state cooling simulations as a function of the MPS's bond dimension, for the integrable TFIM with the parameters used in Figure 3. We show data for both PM and AFM phases at two different bath couplings $\theta = 0.1, 0.05$, and for bond dimensions $d = 100, 150, 200, 250$.

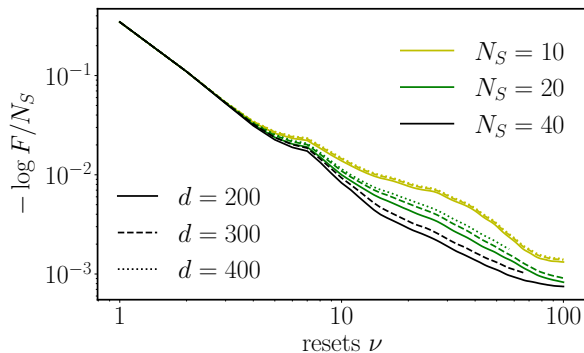


Figure 13. Convergence of ground state cooling simulations as a function of the MPS's bond dimension, for the non-integrable Ising model with the parameters used in Figure 6. Full/dashed/dotted bond dimensions $d = 200, 300, 400$ respectively. For increasing system sizes, there is a small drift with d at $\nu > 10$, but the monotonic increase of fidelity is observed for all bond dimensions.

the nearest-neighbor system-bath channel. Note that the next-nearest-neighbour gate arises from the quasi-1d geometry. This is the most expensive step of the algorithm as it requires two singular value decompositions and scales as $O(\dim(m)^4 d^3)$.

For the simulations with decoherence, following the

unitary channel we apply the decoherence channel Eq. (49) with jump operators in Eq. (54). Finally the reset of auxiliaries is performed by simply modifying the matrix elements of each auxiliary qubit tensor as,

$$\begin{aligned} A_{00s_{i-1}s_i}^i &\rightarrow A_{00s_{i-1}s_i}^i + A_{11s_{i-1}s_i}^i, \\ A_{m \neq 00s_{i-1}s_i}^i &\rightarrow 0. \end{aligned} \quad (\text{E10})$$

In the non-integrable TFIM in the presence of a longitudinal field, the local unitary operations are defined according to Eq. (66), and the rest of the algorithm is unaffected.

Next, we study the effects of truncation due to finite bond dimension during the cooling protocol in Figures 12 and 13. In Fig. 12 we consider the TFIM cooling for the parameters shown in Fig. 3 of the main text. We only show data for two values of the coupling, $\theta = 0.1, 0.05$ for the MCP, since the SCP protocol is well converged for all bond dimensions. We observe that the convergence is slower for the larger coupling, suggesting higher bond dimensions are needed to capture non-perturbative effects. Phenomenologically, such behavior is expected since higher-order in θ corrections are expected to lead processes that are less spatially local, thus requiring a larger bond dimension to be accurately captured.

The comparison of data obtained with different bond dimension $d = 200, 300, 400$ for the non-integrable model is shown in Fig. 13. We note that the bond dimension necessary for convergence depends on the correlation length of the ground state. For the parameters of the TFIM with longitudinal field used in the main text ($h_x = h_z = 0.15, J = 0.1$), the effects of truncation are almost negligible for bond dimension values considered.

Appendix F: Comparison of noisy kinetic equation and MPS simulations

In Section IV we derived the kinetic equation in the presence of noise, Eq. (51), which includes transitions induced by qubit dephasing and decay, Eqs. (51). Here we compare the accuracy of the rate equation predictions against MPS simulations. We focus on the MCP with the same parameters as in Fig. (4), namely finite density of auxiliaries, $N_A = N_S = 20$, and $T = 12 = 2\beta$. In Fig. 14 we plot the quasiparticle densities in the steady state, obtained from the kinetic equation prediction (black dashed line) and MPS simulations (scatter points). We use a maximum MPS bond dimension of $d = 100$ and run the simulations starting from the exact ground state, as described in Section III. We fix the noise strength $\gamma_d = \gamma_\phi = 0.1\theta^2$, and show results for three different coupling strengths, $\theta = 0.2, 0.1, 0.05$, finding good qualitative agreement for the smaller coupling values $\theta = 0.1, 0.05$.

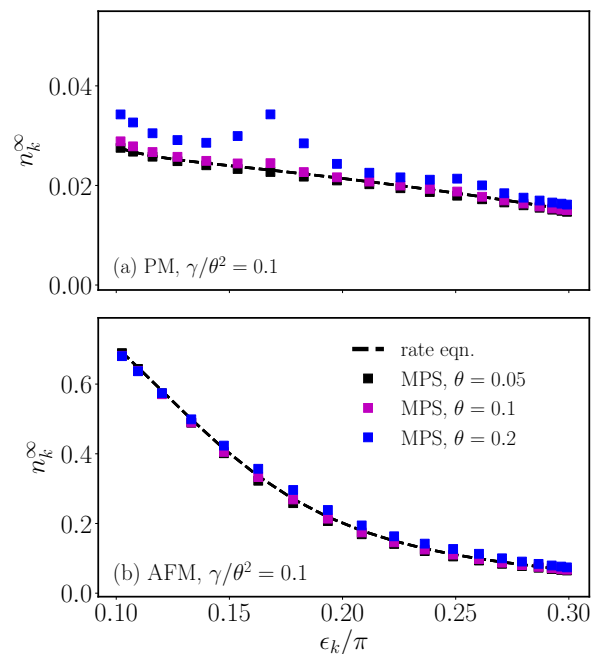


Figure 14. Quasiparticle occupation numbers n_k^∞ in steady state, as a function of quasienergy ϵ_k , for noise strength $\gamma_d = \gamma_\phi = 0.1\theta^2$. (a) PM and (b) AFM phases. Rate equation prediction (dashed line) vs. MPS simulations (points), for three values of the coupling θ . Protocol parameters are as in Fig. (4). The MPS simulations use a maximum bond dimension of $d = 100$.

-
- [1] B. P. Lanyon, J. D. Whitfield, G. G. Gillett, M. E. Goggin, M. P. Almeida, I. Kassal, J. D. Biamonte, M. Mohseni, B. J. Powell, M. Barbieri, *et al.*, Towards quantum chemistry on a quantum computer, *Nature chemistry* **2**, 106 (2010).
- [2] A. Kandala, A. Mezzacapo, K. Temme, M. Takita, M. Brink, J. M. Chow, and J. M. Gambetta, Hardware-efficient variational quantum eigensolver for small molecules and quantum magnets, *nature* **549**, 242 (2017).
- [3] B. Bauer, S. Bravyi, M. Motta, and G. K.-L. Chan, Quantum algorithms for quantum chemistry and quantum materials science, *Chemical Reviews* **120**, 12685 (2020).
- [4] G. A. Quantum, Collaborators*†, F. Arute, K. Arya, R. Babbush, D. Bacon, J. C. Bardin, R. Barends, S. Boixo, M. Broughton, B. B. Buckley, *et al.*, Hartree-fock on a superconducting qubit quantum computer, *Science* **369**, 1084 (2020).
- [5] A. B. Finnila, M. A. Gomez, C. Sebenik, C. Stenson, and J. D. Doll, Quantum annealing: A new method for minimizing multidimensional functions, *Chemical physics letters* **219**, 343 (1994).
- [6] E. Farhi, J. Goldstone, S. Gutmann, J. Lapan, A. Lundgren, and D. Preda, A quantum adiabatic evolution algorithm applied to random instances of an np-complete problem, *Science* **292**, 472 (2001).
- [7] A. Y. Kitaev, Quantum measurements and the abelian stabilizer problem (1995), arXiv:quant-ph/9511026 [quant-ph].
- [8] D. S. Abrams and S. Lloyd, Quantum algorithm providing exponential speed increase for finding eigenvalues and eigenvectors, *Phys. Rev. Lett.* **83**, 5162 (1999).
- [9] E. Farhi, J. Goldstone, S. Gutmann, and M. Sipser, Quantum computation by adiabatic evolution, arXiv preprint quant-ph/0001106 (2000).
- [10] D. Poulin and P. Wocjan, Preparing ground states of quantum many-body systems on a quantum computer, *Phys. Rev. Lett.* **102**, 130503 (2009).
- [11] S. Boixo, E. Knill, and R. D. Somma, Eigenpath traversal by phase randomization, *Quantum Inf. Comput.* **9**, 833 (2009).
- [12] Y. Ge, J. Tura, and J. I. Cirac, Faster ground state preparation and high-precision ground energy estimation with fewer qubits, *Journal of Mathematical Physics* **60**, 022202 (2019).
- [13] J. Preskill, Quantum computing in the nisq era and beyond, *Quantum* **2**, 79 (2018).
- [14] T. Albash and D. A. Lidar, Adiabatic quantum computation, *Reviews of Modern Physics* **90**, 015002 (2018).
- [15] M. Greiner, O. Mandel, T. Esslinger, T. W. Hänsch, and I. Bloch, Quantum phase transition from a superfluid to a mott insulator in a gas of ultracold atoms, *Nature* **415**, 39 (2002).

- [16] J. Simon, W. S. Bakr, R. Ma, M. E. Tai, P. M. Preiss, and M. Greiner, Quantum simulation of antiferromagnetic spin chains in an optical lattice, *Nature* **472**, 307 (2011).
- [17] G. Semeghini, H. Levine, A. Keesling, S. Ebadi, T. T. Wang, D. Bluvstein, R. Verresen, H. Pichler, M. Kalinowski, R. Samajdar, A. Omran, S. Sachdev, A. Vishwanath, M. Greiner, V. Vuletić, and M. D. Lukin, Probing topological spin liquids on a programmable quantum simulator, *Science* **374**, 1242 (2021), <https://www.science.org/doi/pdf/10.1126/science.abi8794>.
- [18] P. Scholl, M. Schuler, H. J. Williams, A. A. Eberharter, D. Barredo, K.-N. Schymik, V. Lienhard, L.-P. Henry, T. C. Lang, T. Lahaye, A. M. Läuchli, and A. Browaeys, Quantum simulation of 2d antiferromagnets with hundreds of rydberg atoms, *Nature* **595**, 233 (2021).
- [19] M. Cerezo, A. Arrasmith, R. Babbush, S. C. Benjamin, S. Endo, K. Fujii, J. R. McClean, K. Mitarai, X. Yuan, L. Cincio, *et al.*, Variational quantum algorithms, *Nature Reviews Physics* **3**, 625 (2021).
- [20] J. Tilly, H. Chen, S. Cao, D. Picozzi, K. Setia, Y. Li, E. Grant, L. Wossnig, I. Rungger, G. H. Booth, and J. Tennyson, The variational quantum eigensolver: A review of methods and best practices, *Physics Reports* **986**, 1 (2022).
- [21] D. A. Fedorov, B. Peng, N. Govind, and Y. Alexeev, Vqe method: a short survey and recent developments, *Materials Theory* **6**, 1 (2022).
- [22] K. Bharti, A. Cervera-Lierta, T. H. Kyaw, T. Haug, S. Alperin-Lea, A. Anand, M. Degroote, H. Heimonen, J. S. Kottmann, T. Menke, W.-K. Mok, S. Sim, L.-C. Kwek, and A. Aspuru-Guzik, Noisy intermediate-scale quantum algorithms, *Rev. Mod. Phys.* **94**, 015004 (2022).
- [23] T. Louvet, T. Ayril, and X. Waintal, Go-no go criteria for performing quantum chemistry calculations on quantum computers (2023), [arXiv:2306.02620](https://arxiv.org/abs/2306.02620) [quant-ph].
- [24] J. R. McClean, S. Boixo, V. N. Smelyanskiy, R. Babbush, and H. Neven, Barren plateaus in quantum neural network training landscapes, *Nature communications* **9**, 4812 (2018).
- [25] S. Wang, E. Fontana, M. Cerezo, K. Sharma, A. Sone, L. Cincio, and P. J. Coles, Noise-induced barren plateaus in variational quantum algorithms, *Nature Communications* **12**, 6961 (2021).
- [26] S. H. Sack, R. A. Medina, A. A. Michailidis, R. Kueng, and M. Serbyn, Avoiding barren plateaus using classical shadows, *PRX Quantum* **3**, 020365 (2022).
- [27] B. M. Terhal and D. P. DiVincenzo, Problem of equilibration and the computation of correlation functions on a quantum computer, *Phys. Rev. A* **61**, 022301 (2000).
- [28] E. B. Davies, Markovian master equations, *Communications in mathematical Physics* **39**, 91 (1974).
- [29] B. Kraus, H. P. Büchler, S. Diehl, A. Kantian, A. Micheli, and P. Zoller, Preparation of entangled states by quantum markov processes, *Phys. Rev. A* **78**, 042307 (2008).
- [30] S. Diehl, A. Micheli, A. Kantian, B. Kraus, H. P. Büchler, and P. Zoller, Quantum states and phases in driven open quantum systems with cold atoms, *Nat. Phys.* **4**, 878 (2008).
- [31] F. Verstraete, M. M. Wolf, and J. Ignacio Cirac, Quantum computation and quantum-state engineering driven by dissipation, *Nat. Phys.* **5**, 633 (2009).
- [32] S. Roy, J. Chalker, I. Gornyi, and Y. Gefen, Measurement-induced steering of quantum systems, *Physical Review Research* **2**, 033347 (2020).
- [33] M. J. Kastoryano and F. G. Brandao, Quantum gibbs samplers: The commuting case, *Communications in Mathematical Physics* **344**, 915 (2016).
- [34] C.-F. Chen, M. J. Kastoryano, F. G. S. L. Brandão, and A. Gilyén, Quantum thermal state preparation (2023), [arXiv:2303.18224](https://arxiv.org/abs/2303.18224) [quant-ph].
- [35] J. T. Barreiro, M. Müller, P. Schindler, D. Nigg, T. Monz, M. Chwalla, M. Hennrich, C. F. Roos, P. Zoller, and R. Blatt, An open-system quantum simulator with trapped ions, *Nature* **470**, 486 (2011).
- [36] Y. Lin, J. P. Gaebler, F. Reiter, T. R. Tan, R. Bowler, A. S. Sørensen, D. Leibfried, and D. J. Wineland, Dissipative production of a maximally entangled steady state of two quantum bits, *Nature* **504**, 415 (2013).
- [37] S. Shankar, M. Hatridge, Z. Leghtas, K. M. Sliwa, A. Narla, U. Vool, S. M. Girvin, L. Frunzio, M. Mirrahimi, and M. H. Devoret, Autonomously stabilized entanglement between two superconducting quantum bits, *Nature* **504**, 419 (2013).
- [38] X. Mi, A. Michailidis, S. Shabani, K. Miao, P. Klimov, J. Lloyd, E. Rosenberg, R. Acharya, I. Aleiner, T. Andersen, *et al.*, Stable quantum-correlated many-body states through engineered dissipation, *Science* **383**, 1332 (2024).
- [39] D. A. Abanin, W. De Roeck, W. W. Ho, and F. Huveneers, Effective Hamiltonians, prethermalization, and slow energy absorption in periodically driven many-body systems, *Physical Review B* **95**, 014112 (2017).
- [40] M. Metcalf, J. E. Moussa, W. A. de Jong, and M. Sarovar, Engineered thermalization and cooling of quantum many-body systems, *Physical Review Research* **2**, 023214 (2020).
- [41] M. Raghunandan, F. Wolf, C. Ospelkaus, P. O. Schmidt, and H. Weimer, Initialization of quantum simulators by sympathetic cooling, *Sci. Adv.* **6**, eaaw9268 (2020).
- [42] S. Polla, Y. Herasymenko, and T. E. O'Brien, Quantum digital cooling, *Phys. Rev. A* **104**, 012414 (2021).
- [43] A. Matthies, M. Rudner, A. Rosch, and E. Berg, Programmable adiabatic demagnetization for systems with trivial and topological excitations (2023), [arXiv:2210.17256](https://arxiv.org/abs/2210.17256) [quant-ph].
- [44] D. A. Puente, F. Motzoi, T. Calarco, G. Morigi, and M. Rizzi, Quantum state preparation via engineered ancilla resetting, [arXiv preprint arXiv:2305.08641](https://arxiv.org/abs/2305.08641) (2023).
- [45] P. Coleman, *Introduction to Many-Body Physics* (Cambridge University Press, 2015).
- [46] E. Lieb, T. Schultz, and D. Mattis, Two soluble models of an antiferromagnetic chain, *Annals of Physics* **16**, 407 (1961).
- [47] S. Sachdev, Quantum phase transitions, *Physics world* **12**, 33 (1999).
- [48] A. A. Ovchinnikov, D. V. Dmitriev, V. Y. Krivnov, and V. O. Cheranovskii, Antiferromagnetic ising chain in a mixed transverse and longitudinal magnetic field, *Phys. Rev. B* **68**, 214406 (2003).
- [49] For protocols considered below, f_τ can be positive or negative, but for this choice the sum $\sum_{\tau=1}^T |f_\tau| \gtrsim 1$.
- [50] H.-P. Breuer and F. Petruccione, *The theory of open quantum systems* (Oxford University Press, USA, 2002).
- [51] D. A. Lidar, Lecture notes on the theory of open quantum systems (2020), [arXiv:1902.00967](https://arxiv.org/abs/1902.00967) [quant-ph].

- [52] We note that the second assumption is practically necessary, as the diagonal assumption still leaves us with $O(\exp(N_S))$ coupled equations to solve.
- [53] M. Rigol, V. Dunjko, V. Yurovsky, and M. Olshanii, Relaxation in a completely integrable many-body quantum system: An ab initio study of the dynamics of the highly excited states of 1d lattice hard-core bosons, *Phys. Rev. Lett.* **98**, 050405 (2007).
- [54] F. Lange, Z. Lenarčič, and A. Rosch, Time-dependent generalized gibbs ensembles in open quantum systems, *Physical Review B* **97**, 165138 (2018).
- [55] We note that the normalization factor is chosen according to the condition $\sum_{\tau=1}^T f_{\tau} = 1$. The modulated coupling in Eq. (29) is sign-changing, however, $\sum_{\tau=1}^T |f_{\tau}|$ is of order 1 for all cases considered below.
- [56] M. Thakurathi, A. A. Patel, D. Sen, and A. Dutta, Floquet generation of majorana end modes and topological invariants, *Phys. Rev. B* **88**, 155133 (2013).
- [57] B. Bauer, T. Pereg-Barnea, T. Karzig, M.-T. Rieder, G. Refael, E. Berg, and Y. Oreg, Topologically protected braiding in a single wire using floquet majorana modes, *Phys. Rev. B* **100**, 041102 (2019).
- [58] A. Leroise, M. Sonner, and D. A. Abanin, Scaling of temporal entanglement in proximity to integrability, *Phys. Rev. B* **104**, 035137 (2021).
- [59] M. Žnidarič, Relaxation times of dissipative many-body quantum systems, *Physical Review E* **92**, 042143 (2015).
- [60] Heating processes, in particular due to noise, may in principle involve a large number of particles; however, we will find that few-quasiparticle processes are dominant, and considering them gives an accurate approximation of heating rates.
- [61] G. B. Mbeng, A. Russomanno, and G. E. Santoro, The quantum ising chain for beginners (2020), arXiv:2009.09208 [quant-ph].
- [62] F. Verstraete, J. J. García-Ripoll, and J. I. Cirac, Matrix product density operators: Simulation of finite-temperature and dissipative systems, *Phys. Rev. Lett.* **93**, 207204 (2004).
- [63] M. Zwolak and G. Vidal, Mixed-state dynamics in one-dimensional quantum lattice systems: A time-dependent superoperator renormalization algorithm, *Phys. Rev. Lett.* **93**, 207205 (2004).
- [64] G. Vidal, Efficient classical simulation of slightly entangled quantum computations, *Physical review letters* **91**, 147902 (2003).
- [65] G. Vidal, Efficient simulation of one-dimensional quantum many-body systems, *Physical review letters* **93**, 040502 (2004).
- [66] M. Fishman, S. R. White, and E. M. Stoudenmire, The ITensor Software Library for Tensor Network Calculations, *SciPost Phys. Codebases*, 4 (2022).
- [67] The steady state can be efficiently found by root-finding algorithms, after the cooling and noise-induced rates have been calculated via Wick's theorem. In practice, the system reaches its steady state quickly and we evolve the rate equation in time until the quasiparticle occupations have effectively converged.
- [68] N. Moll, P. Barkoutsos, L. S. Bishop, J. M. Chow, A. Cross, D. J. Egger, S. Filipp, A. Fuhrer, J. M. Gambetta, M. Ganzhorn, A. Kandala, A. Mezzacapo, P. Müller, W. Riess, G. Salis, J. Smolin, I. Tavernelli, and K. Temme, Quantum optimization using variational algorithms on near-term quantum devices, *Quantum Science and Technology* **3**, 030503 (2018).
- [69] G. Modugno, G. Ferrari, G. Roati, R. J. Brecha, A. Simoni, and M. Inguscio, Bose-einstein condensation of potassium atoms by sympathetic cooling, *Science* **294**, 1320 (2001), <https://www.science.org/doi/pdf/10.1126/science.1066687>.
- [70] J. Kempe, A. Kitaev, and O. Regev, The complexity of the local hamiltonian problem, *Siam journal on computing* **35**, 1070 (2006).
- [71] S. Bravyi, M. B. Hastings, and F. Verstraete, Lieb-robinson bounds and the generation of correlations and topological quantum order, *Physical review letters* **97**, 050401 (2006).
- [72] M. B. Hastings, Topological order at nonzero temperature, *Physical review letters* **107**, 210501 (2011).
- [73] G. Kishony, M. S. Rudner, A. Rosch, and E. Berg, Gauged cooling of topological excitations and emergent fermions on quantum simulators, arXiv preprint arXiv:2310.16082 (2023).
- [74] C.-F. Chen and F. G. Brandao, Fast thermalization from the eigenstate thermalization hypothesis, arXiv preprint arXiv:2112.07646 (2021).
- [75] O. Shtanko and R. Movassagh, Preparing thermal states on noiseless and noisy programmable quantum processors (2023), arXiv:2112.14688 [quant-ph].
- [76] P. Rall, C. Wang, and P. Wocjan, Thermal State Preparation via Rounding Promises, *Quantum* **7**, 1132 (2023).
- [77] N. Iorgov, V. Shadura, and Y. Tykhyy, Spin operator matrix elements in the quantum ising chain: fermion approach, *Journal of Statistical Mechanics: Theory and Experiment* **2011**, P02028 (2011).
- [78] E. Barouch and B. M. McCoy, Statistical mechanics of the x y model. ii. spin-correlation functions, *Physical Review A* **3**, 786 (1971).
- [79] T. Barthel and Y. Zhang, Solving quasi-free and quadratic lindblad master equations for open fermionic and bosonic systems, *Journal of Statistical Mechanics: Theory and Experiment* **2022**, 113101 (2022).
- [80] R. Orús, A practical introduction to tensor networks: Matrix product states and projected entangled pair states, *Annals of physics* **349**, 117 (2014).
- [81] J. C. Bridgeman and C. T. Chubb, Hand-waving and interpretive dance: an introductory course on tensor networks, *Journal of physics A: Mathematical and theoretical* **50**, 223001 (2017).